NOVEL IMPLEMENTATIONS OF PLANAR ANTENNAS WITH GOVERNABLE CIRCULAR POLARIZATION

by

Dip Thakar

A thesis submitted to the faculty of
The University of North Carolina at Charlotte
in partial fulfillment of the requirements
for the degree of Master of Science in
Electrical Engineering

Charlotte

2018

Approved by:

_____

Dr. Ryan Adams

_____

Dr. Thomas Weldon

_____

Dr. Tao Han

ABSTRACT

DIP THAKAR. Novel implementations of planar antennas with governable circular polarization. (Under the direction of DR. RYAN ADAMS)

This document is an explicit and an exclusive account on two antennas. This literature is an attempt to solve some of the challenges for planar antennas in the frequency independent class and exploit the radiative nature of narrow band patch antenna arrays to new capabilities.

The first antenna is a rectangular patch element array with two ports and operates at $5GHz$. The structure is designed to emit circularly polarized waves. The right-handedness or left-handedness of this emitted wave can be changed dynamically by switching the ports. This attribute is coined as "Encrypted Polarization" in this document. The presence of two ports in the design is further exploited to theoretically introduce the idea of using this antenna as a filter element. The measured results show a 6% shift in the operating frequency when compared with the simulated results. It is then proved that a discrepancy in the value of the dielectric constant of the substrate is responsible for this variance.

The second antenna is a modification of a conventional Archimedean Spiral Antenna (ASA). The arms of the spiral are kept on either side of the substrate and the arms of the spiral are wider than a tradiational design. The feed of the antenna is remarkably simplified by introducing the opportunity of attaching the coaxial connector directly at the center of the spiral. A 50Ω input impedance is obtained for the structure because of change in the metal to slot ratio. A simulated bandwidth of $40 : 1$ is obtained with the antenna operating from $700MHz$ to $29.9GHz$. The actual results change the upper limit to $19GHz$. Fabrication limitations in the physical design is assumed to be the root cause for this inconsistency.

ACKNOWLEDGEMENTS

I would like to express my deepest gratitude to my parents, without whom this journey would never have started. Although they have stayed approximately 8100 miles away while this work was executed, I never felt a heartbeat away. I thank them for making me what I am today as a person, supporting me constantly throughout and taking part in all my struggles.

I would like to specially thank my future wife, Ms. Meha Soni who has proven to be my better half in the most stressful times way before our wedding. Her supportive nature and positive attitude has been one of the prime motivations for this work.

A big thank you to all of my friends specifically Ajay Naik and Kathryn Smith for supporting me. Mr. Ajay Naik listened to my dumb ideas all the time while Ms. Kathryn Smith has been my best lab partner so far. She is an inspiration to everyone in the electro-magnetics lab. I bow down to God and thank Him to bless me with all these people.

I also thank Science for always being persistent with its laws. Without it, there is nothing to play with in this infinite cosmos.

DEDICATION

This work is solely dedicated to my advisor, Dr. Ryan Adams, who introduced me to the world of Electro-magnetics and all the magic that lies within.

TABLE OF CONTENTS

LIST OF FIGURES

LIST OF TABLES

LIST OF SYMBOLS

ϵ_e	relative effective dielectric constant of the medium with respect to air
ϵ_r	relative dielectric constant of the medium with respect to air
η_0	impedance of free space
λ_0	wavelength in free space
λ_e	effective wavelength in dielectric medium
ρ_e	electric charge density
ρ_m	magnetic charge density
$\vec{A}$	Vector Magnetic potential
$\vec{B}$	Magnetic Field Density
$\vec{D}$	Electric Field Density
$\vec{E}$	Electric Field Intensity
$\vec{H}$	Magnetic Field Intensity
$\vec{J_e}$	surface electric current density
$\vec{J_m}$	surface magnetic current density
H_{sub}	Dielectric substrate thickness
$HFSS$	High Frequency Structure Simulator

CHAPTER 1: INTRODUCTION

Nikola Tesla has always been my favorite scientist of all time. If I may digress to include one of his quotes here,

> "If you want to find the secrets of the universe, think in terms of energy, frequency and vibration."

As per Einstein, this energy can only be converted from one form to the other. In this world full of antennas, innumerable amount of wireless electromagnetic energy transactions take place, most of them happening intentionally and with the required amount of efficiency. Air or vacuum is usually the medium for propagation for these transactions. Semiconductors and metals are the counterpart wired mediums from where communication occurs. Radiation is a problem for such wired media. For wireless systems, where air is the medium, the signal must satisfy all the properties of an electromagnetic wave in order to travel and radiation is the primary goal. One can say that the radiative property of metals is exploited in order to achieve wireless communication.

Antennas enable a communication system to go wireless. They are basically impedance transformers where they are designed to offer an input impedance of 50Ω ideally to the RF input signal. The antenna structure exhibits an output impedance somewhere in the range of 377Ω, the impedance of free space. Because of this match, it is easier for a wave to radiate in free space or get absorbed by an antenna. Similarly, all the power gets transferred to and from the port of the antenna. The IEEE Standard Definitions of Terms for Antennas (IEEE Std 145-2013) defines an antenna as "That part of a transmitting or receiving system that is designed to radiate or to receive

electromagnetic waves". The signal at the RF input gets converted into an electromagnetic wave with the help of an antenna and gets transmitted to free space because of the impedance match. The case is reverse when the antenna is at the receiving end.

Talking about transmission and reception and since this document deals with a frequency independent antenna, it is imperative to have a knowledge of the various frequency band allocations in the electromagnetic spectrum. This allocation is done based on frequency, or consecutively, the transmitted power. Higher frequency has more power and the wave can travel farther away. This way the communication changes from near ground to satellite. As per Wikipedia, the radio spectrum is the part of the electromagnetic spectrum from 3 Hz to 3000 GHz (3 THz). Electromagnetic waves in this frequency range, called radio waves, are extremely widely used in modern technology, particularly in telecommunication. To prevent interference between different users, the generation and transmission of radio waves is strictly regulated by national laws, coordinated by an international body, the International Telecommunication Union (ITU). The ITU radio bands are designations defined in the ITU Radio Regulations. Article 2, provision No. 2.1 states that "the radio spectrum shall be subdivided into nine frequency bands, which shall be designated by progressive whole numbers in accordance with Table 1.1. Note that the last column does not form part of the table in Provision No. 2.1 of the Radio Regulations. The table originated with a recommendation of the IVth CCIR meeting, held in Bucharest in 1937, and was approved by the International Radio Conference held at Atlantic City, NJ in 1947. The idea to give each band a number, in which the number is the logarithm of the approximate geometric mean of the upper and lower band limits in Hz, originated with B.C. Fleming-Williams, who suggested it in a letter to the editor of Wireless Engineer in 1942. (For example, the approximate geometric mean of Band 7 is 10 MHz, or 10^7 Hz.)

Table 1.1: Table of ITU radio bands

Band number	**Abbreviation**	**Frequency range**	**Wavelength range**
4	VLF	3 to 30 kHz	10 to 100 km
5	LF	30 to 300 kHz	1 to 10 km
6	MF	300 to 3000 kHz	100 to 1000 m
7	HF	3 to 30 MHz	10 to 100 m
8	VHF	30 to 300 MHz	1 to 10 m
9	UHF	300 to 3000MHz	10 to 100 cm
10	SHF	3 to 30 GHz	1 to 10 cm
11	EHF	30 to 300 GHz	1 to 10 mm
12	THF	300 to 3000 GHz	0.1 to 1 mm

The IEEE standard has different frequency designations and there are unique band names too. Table 1.2 summarizes the radar-frequency bands as per the IEEE standard.

1.1 A brief history on Antennas

This goes back to 1885-1886 when Heinrich R. Hertz demonstrated the generation of radio waves at UHF using a gap dipole at Karlsruhe University, Germany [1]. Hertz was able to detect radio waves 20 m away using a high-voltage electrical spark discharge to excite the dipole gap. From recorded conversations, Hertz did not seem to understand the impact of his experiments, but instead did a validation of newly developed Maxwell's equations. Within 10 years, Nikola Tesla at the Franklin Institute in the U.S., Marconi in Bologna, Italy, Popov in Russia, and Bose in India, demonstrated wireless telegraphy. In 1892, Tesla delivered a widely distributed presentation at the IRE of London about "transmitting intelligence without wires," and in 1895, he transmitted signals which were detected 50 miles (80 km) away. Concurrently in 1894, Bose used wireless signals to ring a bell in Kolkata, and Popov presented his

radio receiver to the Russian Physical and Chemical Society on May 7, 1895.

Table 1.2: Table of IEEE radio bands

Band designation	**Frequency range**	**Comments**
HF	0.003 to 0.03 GHz	High Frequency
VHF	0.03 to 0.3 GHz	Very High Frequency
UHF	0.3 to 1 GHz	Ultra High Frequency
L	1 to 2 GHz	Long wave
S	2 to 4 GHz	Short wave
C	4 to 8 GHz	Compromise between S and X
X	8 to 12 GHz	Used in WW II for fire control.
K_u	12 to 18 GHz	Kurz-under
K	18 to 27 GHz	Kurz (German for "short")
K_a	27 to 40 GHz	Kurz-above
V	40 to 75 GHz	
W	75 to 110 GHz	W follows V in the alphabet
mm or G	110 to 300 GHz	Millimeter

Marconi is certainly considered the key individual for his contributions to the commercialization of radio waves, and he received a Nobel prize for his work in 1909. Nevertheless, Marconi's widely advertised first radio wave transmission experiment was in 1895, and his British patent application in 1897 was preceded by that of Tesla. A culmination of Marconi's experiments was the December 12, 1901 trans-Atlantic radio wave transmission of the Morse code for letter S. The success of this experiment is often disputed, possibly due to strong atmospheric noise during the time of the experiment, but by the 1920s the U.S. had hundreds of radio stations, and in 1922, the BBC began transmitting in England. Subsequent development of radio detectors,

vacuum tubes, and the tiny transistor in 1947 played a critical role in the practical everyday use of radio waves for communication and wireless transmission of information.

1.2 The Electromagnetics behind Antennas

The electromagnetic theory for Antennas starts with Maxwell's equations. They have a slightly different form here since it is assumed that magnetic charge exists along with all of its associated phenomena. The governing Maxwell's equations for antennas are expressed in 1.1 through 1.4.

$$\nabla \cdot B = \rho_m \tag{1.1}$$

$$\nabla \times \vec{E} = -\frac{\partial \vec{B}}{\partial t} - \vec{J_m} \tag{1.2}$$

$$\nabla \times \vec{H} = \frac{\partial \vec{D}}{\partial t} + \vec{J_e} \tag{1.3}$$

$$\nabla \cdot \vec{D} = \rho_e \tag{1.4}$$

Here ρ_m is the equivalent magnetic charge density while $\vec{J_m}$ denotes the equivalent magnetic current density. These two terms only exist analytically to balance the mathematical model formed from the Maxwell's equations. The other symbols have their usual meanings. Terms like a Permanent Magnetic Conductor (PMC) and Permanent Electric Conductor (PEC) are frequently used in theoretical models to explain the behavior of electric and magnetic currents on the boundaries. For a PMC, $\vec{J_m}, \rho_m \to \infty$ while for a PEC $\vec{J_e}, \rho_e \to \infty$.

The intensity and phase of currents are very important parameters for antennas since moving charges in space and time give rise to far fields. The associated electric and magnetic fields form the radiated electromagnetic wave which is then received by an antenna on the receiving side. There are three important observations regarding the

far fields. The electric field is perpendicular to the magnetic field and the ratio of $\vec{E}$ to $\vec{H}$ is equal to the impedance of free space (η). The radiated power density is in the same direction of propagation of the wave, also denoted by $\vec{k}$. For Transverse Electro-Magnetic (TEM) wave propagation, these far fields decay inversely with the distance from the source of radiation.

1.3 Outline of this work

Before giving a summary on what has been done, it is important to realize where this work stands in a typical transceiver system. After all, antennas can be of no use without a radio. Figure 1.1 shows an over-simplified block diagram of a direct conversion receiver. The RF input signal received from the antenna first passes through a Low Noise Amplifier (LNA) and is fed to two mixer blocks. The function of a mixer is to convert the high frequency modulated input signal to near DC with the help of a Local Oscillator (LO). The low pass filters and the voltage gain amplifiers after the mixer block provide two sets of baseband data. Since the second mixer has the LO frequency phase shifted by 90°, the two sets of data have the in-phase as well as the quadrature-phase components. This scheme enables one to extract complete information from the input RF signal through the antenna.

As highlighted, the work carried out in this document belongs to the antenna block on the top left of the figure. Although as it is described later in this text, the applications for this work are not limited to just the highlighted block in the diagram. The two port patch element array, for example, can be used as a bandpass filter in any intermediate state in the design. Also, the modified archimedean spiral antenna (ASA) developed here if used in the block diagram, can make the radio receiver extremely wideband.

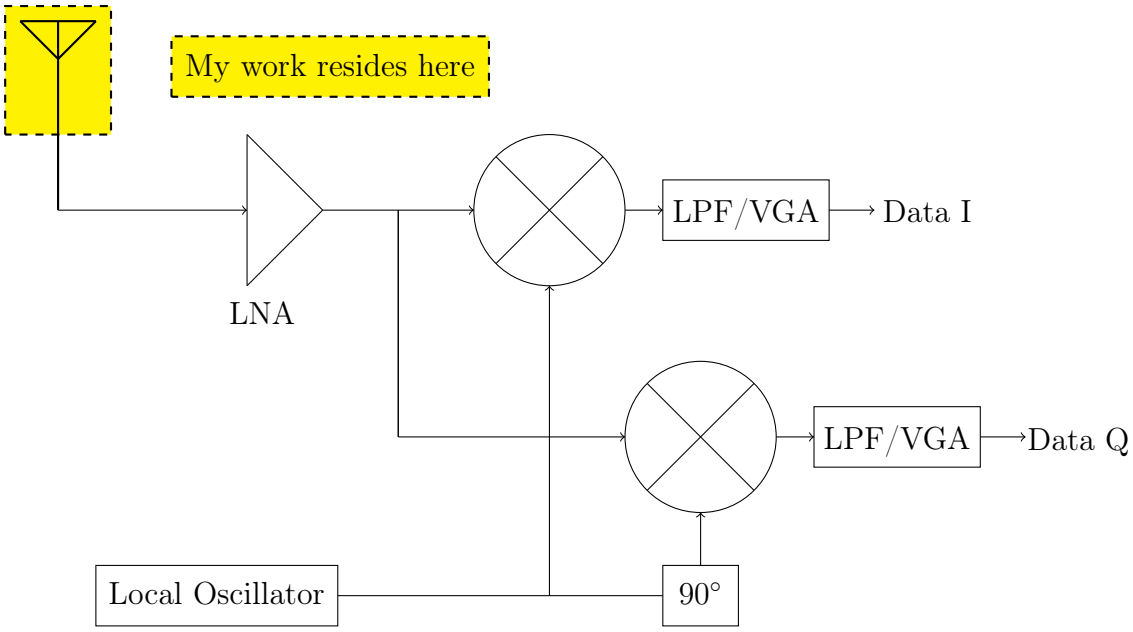

Figure 1.1: Block diagram of a typical direct conversion receiver

All the work presented here has been inspired from the lectures on Antennas delivered by Dr. Ryan Adams at The University of North Carolina at Charlotte. As a matter of fact, the ideas originated in the form of doubts that were asked in some of the lectures. These antennas were intended to be a part of the projects assigned to students in the course and have manifested as a master's thesis over time. Although there has been evidence of similar work done before [2], none of it has been of any influence for this literature in any way.

With humans, antennas have come a long way. Depending on the bandwidth of frequencies supported, antennas are classified into narrow-band, broad-band and frequency independent. Narrow-band response comes from resonance in the physical structure at a particular frequency. The patch antenna array discussed here is an example of a narrow band antenna. Any antenna that supports a broader band of frequencies than a narrow-band antenna can be termed as broad-band. Frequency independent is a different class of antennas altogether spanning a wide range of frequencies of the order of 10:1 bandwidth and they work based on the Rumsey's principle

[3]. The archimedean spiral antenna discussed later in this text falls in this category. The structure of this document has been kept very lucid where it builds a foundation with the theories involved and proceeds with the actual work. Chapter 2 outlines the theory behind both the antennas. The section explains why the antennas have their specific design equations and all the assumptions that go with them. The treatment is purely mathematical. The microstrip patch antennas are introduced first. The phenomenon of fringing associated with a microstrip structure is also discussed. As it will be apparently clear later, it is due to the fringing fields that the patch antenna radiates. The changes to be done in the length and the operating frequency due to the effects of fringing are shown. Polarization is explained next based on its definition in IEEE. This is one of the most important concepts to be acquainted with for this text. One of the important features of the patch antenna array discussed here deals with polarization where the radiated wave can be kept left-handed circularly polarized for some specified amount of time and right-handed circularly polarized for the remainder time. Polarization is switchable and controllable. This has been possible because the antenna has two ports, each port governing the individual states of polarization. All the applications of the patch antenna array have been possible because of the fact that the antenna has two ports. I then share my personal opinion on frequency independence in the next section. The general theory of the frequency independent antennas is then discussed which explains the mathematics involved in Rumsey's principle. A personal intuitive understanding of an archimedean spiral antenna is also added which assumes that a spiral antenna can be thought of as innumerable dipole antennas stacked together. The section ends with a note on how to put this accumulated theory to practice.

Chapters 3 and 4 are dedicated to the work done on making the individual antennas. Chapter 3 starts with applications of the two port four element patch antenna array and continues with its synthesis. The feed of the four element two port patch antenna

array played a crucial role in making the design work the way it should, and hence there is a different section dedicated to the selection process of the feed. Simulation design and results are then shared which provide information on the simulation model designed in HFSS (High Frequency Structure Simulator). HFSS is a finite element method solver for electromagnetic structures developed by Ansys. Results after fabrication are then summarized. Chapter 4 discussed the modified archimedean spiral antenna. This chapter starts, again, with the applications of the antenna, discusses in detail the simulation model prepared and makes way for the actual fabrication scenario. The modifications done on the conventional design are mentioned throughout the chapter which improve the usability of the antenna.

Although the idea behind making these antennas trace back to the lectures in Fall 2016 semester, the designs are far different than what they intended to be. As a fun fact, the four element two port patch antenna array was devised in an attempt to save board space by curving the straight feed into a circle. The idea of adding an extra port was added later to simplify the port switching mechanism. The Archimedean spiral antenna feed had various design strategies in place that can give a good impedance match. In the end it turned out that just by extrapolating the spiral arms into the center and changing the width of the arms did the job.

1.4 Literature survey

Considerable amount of work has been done on improving the performance and usability of Archimedean spirals. One such work presented in [2] is similar to what is described here. The arms of the spiral are placed on either sides of the substrate and the material used is foam instead of FR-4. The text prefers to use double arm width such that if the arms are placed on the same side of the substrate, it will create a short circuit. The modification described in the text here shows that going that far is not necessary. One can leave a gap between the arms and still achieve an excellent impedance match. Tapering is also carried out at the ends of the arms

of the spiral to reduce reflections in [2]. In this text, it has not been tested on how much improvement does tapering provide in terms of performance. The citation has 4.5 turns compared to 15 turns in this design. As a result, the design presented here has absence of reflected currents and subsequently, tapering. The bandwidth of the spiral antenna obtained is $10:1$. The work focuses more on the effect of changing the width of the arms and the height of the substrate on performance. As per the results of the cited work, an arm width of $4mm$ and a substrate height of $1.6mm$ is the best case.

Regarding the feed structure at the center of the spiral, authors in [4] have used a tapered transmission line to match the input impedance. While addressing the issue of impedance matching for the modified ASA in this text, using a tapered transformer feed was considered as an option. Later on, continuing with the same width of the spiral arms till the center worked. Another work carried out related to the effects of the dielectric substrate material on an ASA is discussed [5]. The results from this literature show that with the increase in the value of dielectric permittivity ϵ_r, the performance of a conventional ASA in terms of return loss, axial ratio, efficiency and gain deteriorates. The structural behavior of the modified ASA is different because of the offset in position of the arms. Instead of the reactive part of input impedance being inductive in nature, the modified ASA is capacitive. There is no ground plane used at the bottom of the spiral as shown by the authors in the cited text. Hence, even though the results in [5] are noteworthy, it may not be extremely useful in this case. Since this option required the tapered transmission lines to be on either sides of the substrate, one cannot use the equations of a microstrip line to calculate the appropriate widths for the perfect impedance match. For this, work done on double-sided parallel-strip lines (DSPSL) [6] is essential since the structure formed is primarily a parallel strip line with metal on either sides.

Shifting our focus to the work done on patch antenna arrays, one can start by stating

the fact that the antenna developed in this text has two ports. As of now, there is no evidence of work done in this direction. There have been instances where the patch antenna arrays achieve circular polarization using a parallel feed [7]. The authors have used slot antennas instead of patches and have maintained circular polarization by feeding the slots at different angles. There are four elements used in each array and the sum of all the angles is designed to be 360°. This condition is a necessity for circular polarization and has been followed in this text too. An important note about parallel-fed arrays, as also seen from the cited text, is that the structure requires power dividers along with impedance matching transformers. For series-fed arrays, the community has so far focused on through element design where thought has been given on proper impedance matching of the structure either by changing the transmission line feed widths or by modifying the widths of the patches itself along the array to improve overall directivity of the antenna [8]. Polarization has not been discussed in the cited text. A useful account of the varieties of series feed methods of the patch antenna arrays has been discussed in [9]. Offset series-fed patch arrays do not require power dividers. One can achieve acceptable directivity of the overall array without changing the widths of either the transmission line or the patches. These are called resonant arrays. Another advantage is related to polarization where the shape of the feed can be amended so that the structure can natively emit circularly polarized waves. This text serves as a proof for the above statement.

CHAPTER 2: THEORY ON THE PATCH AND THE ARCHIMEDEAN SPIRAL ANTENNAS

2.1 Theory on the microstrip patch antennas

The microstrip patch antennas are easy to fabricate and integrate with the modern technologies. They are based on the resonant cavity model and are a natural extension to microstrip lines. The structure consists of a feed and a radiating element. The feed can be a microstrip, coaxial or a probe feed. The radiating element can take any size and shape to make the antenna radiative at the frequency of interest. A problem we face with these antennas are surface wave modes which make them less efficient. If the dielectric constant of the substrate is too big, the wave will couple just to that surface, will stay in the dielectric and the antenna will not radiate effectively. Truncated ground plane also gives rise to surface waves which end up radiating but distort the radiation pattern. A high dielectric constant will essentially incline the model towards a dielectric slab waveguide. So, small ϵ_r is desirable for the dielectric substrate. Other recommended parameters are:

- The metal thickness should be very small. It should be negligible compared to the operating wavelength (λ_0) in free space.
- The substrate thickness ($Hsub$) has a trade off and it should typically be in the range $0.003\lambda_0 < Hsub < 0.05\lambda_0$. Higher thickness may make the antenna radiate more but the microstrip feed will also start radiating if fed through it.
- The antenna size should be in the range $\frac{\lambda_0}{3}$ to $\frac{\lambda_0}{2}$. Antenna size tends to decrease with an increase in the dielectric thickness and we thus have an engineering trade-off here as well.

2.1.1 Analysis of the rectangular cavity

The structure of a rectangular patch antenna fed with a microstrip line is shown from two different perspectives in figures 2.1 and 2.2. Notice the fringing fields in Figure 2.2.

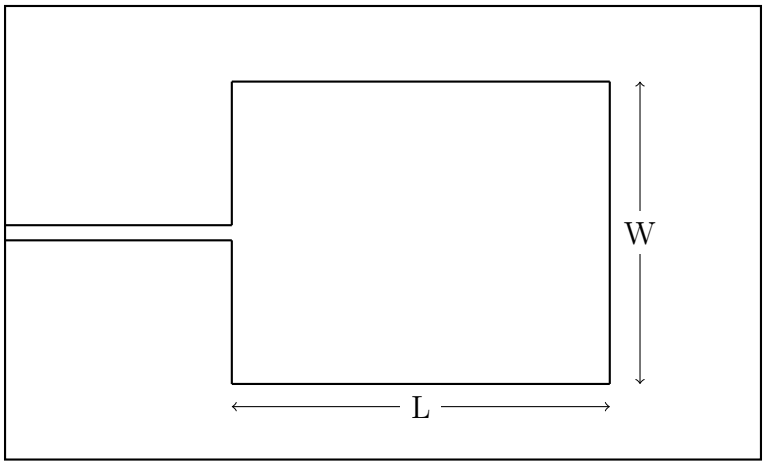

Figure 2.1: Top view of a rectangular patch antenna fed with a microstrip line

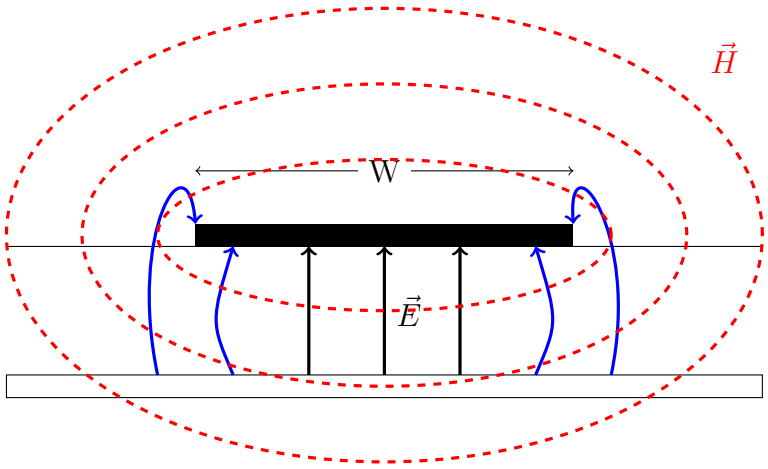

Figure 2.2: Cross section view of a rectangular patch antenna shown in Figure 2.1 with imaginary electric and magnetic field lines. The fringing fields are colored with blue

If the fringing is ignored, the patch antenna model can be assumed to be a cavity with PEC walls on the top and bottom, PMC walls on the sides and filled with a material having ϵ_r as its dielectric constant. This is shown in Figure 2.4.

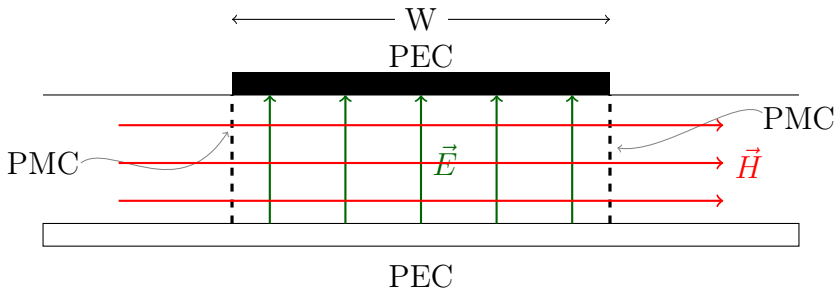

Figure 2.3: Cross section view of a rectangular patch with imaginary electric and magnetic field lines ignoring the fringing fields. The PEC boundaries are labeled on the top and bottom of the cavity while the PMC boundaries are shown with dashed lines

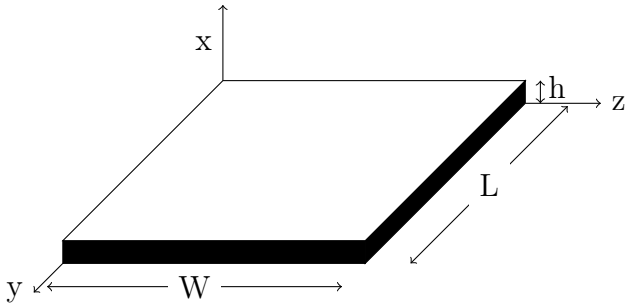

Figure 2.4: The 3D mathematical model of the patch cavity model. The side faces covered in black are assumed to be PMC while the top and bottom faces in white are PEC

If the height h of the dielectric material is fairly smaller than the operating free space wavelength λ_0, it is safe to assume that the magnetic field will only have a horizontal component as shown in Figure 2.3 and the patch model boundary conditions will not be violated. The TM^x solutions are only allowed. [10]

$$\vec{H} = \frac{1}{\mu}\nabla \times \vec{A} = \frac{1}{\mu}\left[\left(\frac{\partial A_z}{\partial y} - \frac{\partial A_y}{\partial z}\right)\hat{a_x} + \left(\frac{\partial A_x}{\partial z} - \frac{\partial A_z}{\partial x}\right)\hat{a_y} + \left(\frac{\partial A_y}{\partial x} - \frac{\partial A_x}{\partial y}\right)\hat{a_z}\right]$$

For enforcing TM^x since $A_y = 0$ and $A_z = 0$,

$$\vec{H} = \frac{\partial A_x}{\partial z}\hat{a_y} - \frac{\partial A_x}{\partial y}\hat{a_z} \tag{2.1}$$

The Ampere's law for TM^x is then,

$$\begin{aligned} \frac{\partial H_z}{\partial y} - \frac{\partial H_y}{\partial z} &= j\omega\epsilon E_x \\ -\frac{\partial H_z}{\partial x} &= j\omega\epsilon E_y \\ \frac{\partial H_y}{\partial x} &= j\omega\epsilon E_z \end{aligned}$$

One can find the electric field components from the magnetic field and the vector magnetic potential. Substituting values from Equation 2.1 and rearranging terms, the electric field components become available.

$$\begin{aligned} E_x = \frac{1}{j\omega\epsilon}\left[-\frac{1}{\mu}\frac{\partial^2 A_x}{\partial y^2} - \frac{1}{\mu}\frac{\partial^2 A_x}{\partial z^2}\right] \\ E_y = \frac{1}{j\omega\mu\epsilon}\frac{\partial^2 A_x}{\partial x \partial y} \\ E_z = \frac{1}{j\omega\mu\epsilon}\frac{\partial^2 A_x}{\partial x \partial z} \end{aligned}$$

The general form of the differential equation at hand which needs to be solved is the Helmholtz equation $\nabla^2\vec{A} + k^2\vec{A} = 0$ where $k^2 = {k_x}^2 + {k_y}^2 + {k_z}^2$. The general form of solution of the Helmholtz equation is as stated in 2.2.

$$\begin{aligned} A_x = &[A_1 cos(k_x x) + B_1 sin(k_x x)] \\ &\times [A_2 cos(k_y y) + B_2 sin(k_y y)] \\ &\times [A_3 cos(k_z z) + B_3 sin(k_z z)] \end{aligned} \tag{2.2}$$

In order to generate a valid solution to Equation 2.2, one must impose the necessary boundary conditions on the electric field and the magnetic field components. The treatment is done in this way to take into account the presence of PEC and PMC

walls in the model. For example, a tangential component of electric field cannot exist on a PEC boundary and similarly a PMC surface cannot have a tangential component of the magnetic field. In this sense referring to Figure 2.4, the patch antenna cavity model can have the following boundary conditions on the electric and the magnetic fields:

1. $H_x(x,0,z) = H_z(x,0,z) = 0$
2. $H_x(x,L,z) = H_z(x,L,z) = 0$
3. $H_x(x,y,0) = H_y(x,y,0) = 0$
4. $H_x(x,0,z) = H_y(x,0,z) = 0$
5. $E_y(0,y,z) = E_z(0,y,z) = 0$
6. $E_y(h,y,z) = E_z(h,y,z) = 0$

Using the first boundary condition in 2.2 for $y = 0$ the coefficient $B_2 = 0$. Hence $A_x = Acos(k_x x)cos(k_y y)cos(k_z z)$

Using the second boundary condition, for $y = L$, one obtains $k_y L = n\pi$ where $n = 0, 1, 2....$ Hence,

$$k_y = \frac{n\pi}{L}, n = 0, 1, 2... \tag{2.3}$$

Similarly we get,

$$k_x = \frac{m\pi}{h}, m = 0, 1, 2... \tag{2.4}$$

$$k_z = \frac{p\pi}{W}, p = 0, 1, 2... \tag{2.5}$$

Using these values of k_x, k_y, k_z in 2.2, one has

$$A_x = \sum_{m=0}^{\infty}\sum_{n=0}^{\infty}\sum_{p=0}^{\infty} A_{mnp} cos\left(\frac{m\pi}{h}x\right) cos\left(\frac{n\pi}{L}y\right) cos\left(\frac{p\pi}{W}z\right) \tag{2.6}$$

Since $k^2 = {k_x}^2 + {k_y}^2 + {k_z}^2 = \omega^2\mu\epsilon$, the resonant frequencies of operation of the cavity are,

$$f = \frac{1}{2\pi\sqrt{\mu\epsilon}}\sqrt{\left(\frac{m\pi}{h}\right)^2 + \left(\frac{n\pi}{L}\right)^2 + \left(\frac{p\pi}{W}\right)^2} \tag{2.7}$$

Mathematically it is apparent now why the patch antennas are narrow band. In real world if this model holds, there will be only a discrete set of resonant frequency points.

The dominant mode for this cavity will be when $L > W$ to have $n = 1$ alone. If the width is bigger than the length of the radiating element, there can be other lower modes of operation. The condition $L > W$ ensures that one has a single mode of propagation.

$$f_{010} = \frac{1}{2L\sqrt{\mu\epsilon}} \tag{2.8}$$

This electromagnetic wave trapped inside this cavity has associated $\vec{E}$ and $\vec{H}$ fields. Although PEC is hard boundary and no fields can radiate out from them, on PMC, one can get an effective current density. This can be used to find the far fields of the antenna. The fringing fields on the PEC boundary have surface currents associated with them but since they are negligible compared to the effective current densities on the PMC, the far-field effects of these currents can be ignored. It is assumed that the radiation occurs only due to the currents $\vec{J_{es}}$ and $\vec{J_{ms}}$ shown in Figure 2.5. This can be solved through the method of images.

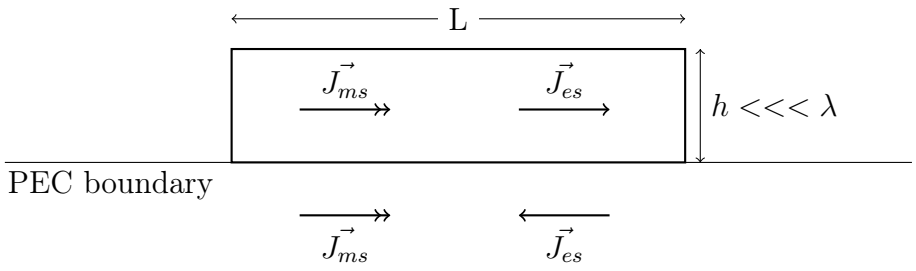

Figure 2.5: The image problem for the surface current densities in microstrip patch cavity model

The electric currents cancel vectorially due to the PEC boundary while the magnetic currents add up. For this image problem the net effective current is, $2\vec{J_{ms}} = 2\vec{E_s} \times \hat{a_n}$ For the dominant mode, $m = 0, n = 1, p = 0$ one has the vector magnetic potential

$$A_x = A_{010} cos\left(\frac{\pi}{L} y\right)$$

which implies that one can obtain the electric and magnetic field components through substitution

$$E_x = -j\omega A_{010} cos\left(\frac{\pi}{L} y\right) \tag{2.9}$$

$$H_z = \frac{\pi}{\mu L} A_{010} sin\left(\frac{\pi}{L} y\right) \tag{2.10}$$

Referring to Figure 2.4, using 2.9 and 2.1.1,
on $y = 0$ face

$$\begin{aligned} \vec{J_{ms}} &= (-j\omega A_{010}\hat{a_x}) \times (-\hat{a_y}) \\ &= j\omega A_{010}\hat{a_z} \end{aligned}$$

and on $y = L$ face

$$\begin{aligned} \vec{J_{ms}} &= (-j\omega A_{010} cos(\pi)\hat{a_x}) \times \hat{a_y} \\ &= j\omega A_{010}\hat{a_z} \end{aligned}$$

Hence, $y = 0$ and $y = L$ faces have identical currents separated by a distance L.

Similarly for $z = 0$ face

$$\begin{aligned}\vec{J_{ms}} &= (-j\omega A_{010} cos\left(\frac{\pi}{L}\right) y\hat{a_x}) \times (-\hat{a_z}) \\ &= -j\omega A_{010} cos\left(\frac{\pi}{L}\right) \hat{a_y}\end{aligned}$$

and on $z = W$ face

$$\begin{aligned}\vec{J_{ms}} &= (-j\omega A_{010} cos\left(\frac{\pi}{L}\right) y\hat{a_x}) \times (-\hat{a_z}) \\ &= j\omega A_{010} cos\left(\frac{\pi}{L}\right) \hat{a_y}\end{aligned}$$

Figure 2.6 shows these currents and from their orientation and magnitudes, it is evident that the faces $y = 0$ and $y = L$ are radiative, since the currents add up. The $z = 0$ and $z = W$ faces negligibly contribute to radiation since they are zero at the center. One can now realize the significance of adding magnetic current density and magnetic charge density in Maxwell's equations. Without these terms, it would be impossible to explain the working of the patch model mathematically.

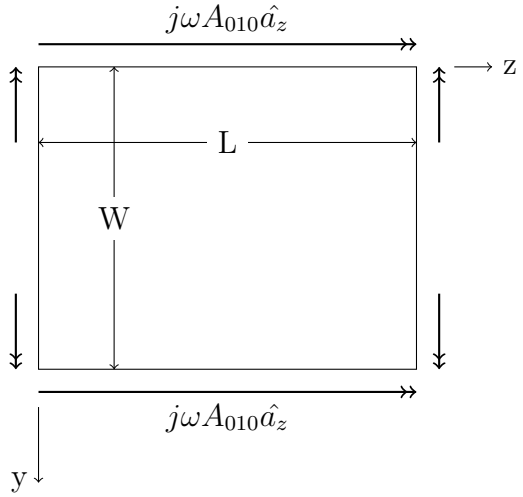

Figure 2.6: The radiative and non-radiative currents on the slots of the patch

It is now an aperture problem as shown in Figure 2.7.

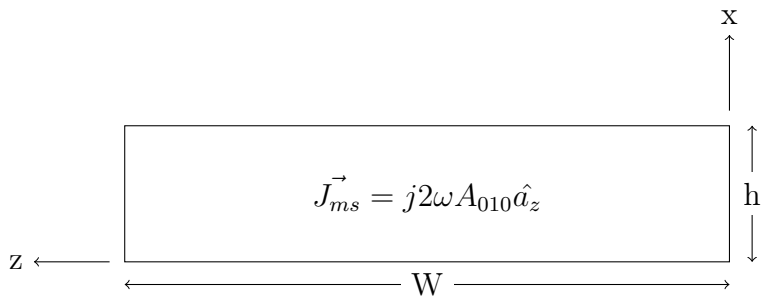

Figure 2.7: Viewing the patch mathematically as an aperture problem

The Electric vector potential over the surface s is given by,

$$\vec{F} = \frac{\epsilon}{4\pi}\int_s \frac{\vec{J_{ms}}}{|\vec{r}-\vec{r'}|}e^{-jk|\vec{r}-\vec{r'}|}ds \tag{2.11}$$

Taking the analysis from [10] and solving the problem directly,

$$E_\theta = \frac{-jke^{-jkr}}{4\pi r}[L_\phi + \eta N_\theta]$$

$$E_\phi = \frac{-jke^{-jkr}}{4\pi r}[L_\theta i\eta N_\theta]$$

Conveniently here $\vec{N} = 0$ as there are no electric currents. Also for L_ϕ

$$L_\phi = \int[-J_{mx}sin\phi + J_{my}cos\phi] = 0$$

since $J_{mx} = J_{my} = 0$. This implies $E_\theta = 0$

$$\begin{aligned} L_\theta &= \int -J_{mz}sin\theta e^{jkr'}cos\psi' ds' \\ &= \int_0^W \int_0^x -j2wA_{010}sin\theta e^{-jkr}cos\psi' dxdz \end{aligned}$$

Hence in the far field the radiation pattern is dictated by 2.12,

$$E_\phi = \frac{jk_0hWA_{010}e^{-jk_0r}}{2\pi r}sin\theta\left[\frac{sinX}{X}\frac{sinZ}{Z}\right] \tag{2.12}$$

where

$$X = \frac{k_0 h}{2} sin\theta cos\phi$$

$$Z = \frac{k_0 W}{2} cos\theta$$

It is important to note that k_0 is the wave number in free space and not in the dielectric medium.

2.1.2 Forever Fringing

Microstrip structure has fringing associated with it. When dealing with the length in a microstrip, one has to adjust the physical length to compensate for the fact that one will see fringing on the outer edge of the microstrip. These adjustments can be made on the value of the relative dielectric constant ϵ_r. Due to fringing , there is an effective additional length ΔL associated on the boundaries along with the actual physical length as shown in Figure 2.8. The effective length is $L_e = L + 2 \times \Delta L$

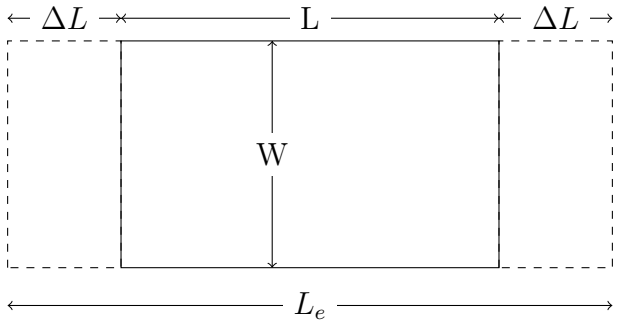

Figure 2.8: Additional length associated with the radiating element due to fringing fields

There is an approximate curve fitted equation that can determine this additional length. If h is the height of the dielectric material,

$$\frac{\Delta L}{h} = 0.412 \frac{(\epsilon_e + 0.3)(\frac{W}{h} + 0.264)}{(\epsilon_e - 0.258)(\frac{W}{h} + 0.8)} \tag{2.13}$$

In order to account for fringing, 2.8 can be more accurately described as

$$fr_{e010} = \frac{1}{2(L + \Delta L)\sqrt{\mu_0 \epsilon_0}\sqrt{\epsilon_e}} \tag{2.14}$$

2.2 Different patch shapes and patch array feed styles

There has been literature backed with similar cavity model theories [11], [12], [13] to prove that patches with a triangular, a circular and as a natural extension to the theory in the previous section, a square shape work. As long as there is an acceptable approximation to the cavity model, the patch shape should work. Hence one has a lot of options on selecting the desired patch shape.

Several patches can be placed together to form an array. It turns out that microstrip arrays can be broken down into three types. These are summarized below:

- In-line series feed: In this case the patches are essentially connected in series through a microstrip transmission line. Along with knowing the lengths and widths of individual patches, one must also decide the distance between the neighboring patch elements in order for the design to work properly. This is shown in figure 2.9.

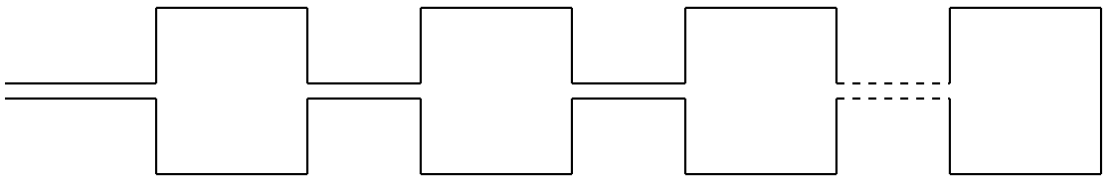

Figure 2.9: In-line series feed design of the microstrip patch antenna array

If the structure of this scheme is viewed as a microstrip transmission line with changing widths along the way, one will observe that there will be an impedance mismatch at every patch element. Standing waves can be observed between the neighboring elements. Based on this thought, the series feed is of two types.

1. Resonant array: These have an impedance mismatch at each antenna el-

ement. This is used as an advantage. The radiation is always broadside. Performance is very narrow-band. It is basically an overlapped resonance of individual elements lined up together.

2. Traveling wave array: This is a different class of antenna which are electrically large. The impedances are matched to the antenna and the feed line. In this array at the last antenna, extra energy may be present. A matched termination and quarter wave transformers are generally added to avoid reflections.

- Out-of-line series feed: The patches are still in series but they are fed with an offset as shown in Figure 2.10. Here, along with deciding the lengths and widths of each element and the distance between neighboring patch elements, one must also decide on the length of the out-of-line offset of the patches. Some of these lengths do not have definite equations and may require trial and error to reach higher efficiency in terms of gain and S_{11}.

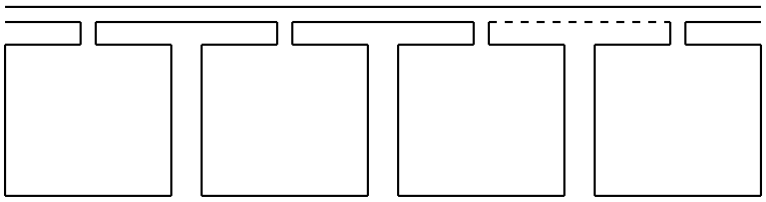

Figure 2.10: Out-of-line series feed design of the microstrip patch antenna array

It is clear that the pattern associated with the in-line series feed and the out-of-line series feed structures will be very different. For the in-line series feed, the pattern in the direction of the progression of the patches will be narrower since the antenna is bigger in this direction. This is the E-field direction. The pattern in the H-field direction perpendicular to the E-field will stay the same approximately, since the antenna width has not changed much. The out-of-line series feed will be different where the E-field direction will have a wider beam

compared to the H-field.

- Parallel feed: As suggested by the name, the patches are fed in a parallel fashion as shown in Figure 2.11 where the power is divided among the patches. Generally there is an equal distribution of power as it generally employs Wilkinson power dividers and quarter wave transformers in the design.

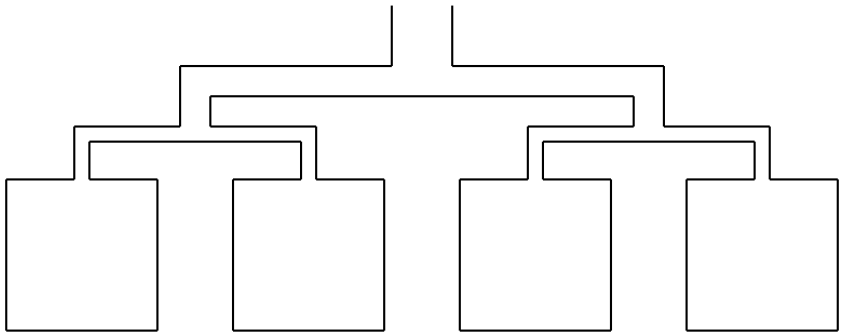

Figure 2.11: Parallel feed design of the microstrip patch antenna array

The patch elements in all these styles can have different sizes [8] and shapes but generally they are identical and the structure is meant to increase the overall gain.

2.3 Polarization principles

For efficient communication, one needs to know what direction the electric field is pointing for the propagating wave. As per IEEE [14], polarization describes the time-varying behavior of $\vec{E}$ on a given plane in space. Depending on the change of direction of the electric field, the polarization can be of various types.

- Linear polarization is when the electric field $\vec{E}$ varies in the same or opposite direction as shown in Figure 2.12

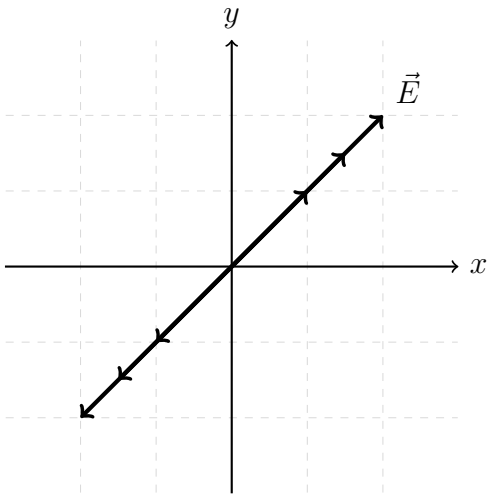

Figure 2.12: An illustration of the variation of electric field with time in the case of linear polarization on the $z = 0$ plane

. Propagation is assumed to be coming in or going out of this page perpendicularly.

- Elliptical polarization is when $\vec{E}$ changes its magnitude and direction with the advancement in time as shown in Figure 2.13. Propagation is again assumed to be coming in or going out of this page perpendicularly. Elliptical polarization is of two types depending on whether the electric field vector traverses the path clockwise or anti-clockwise.

  Right-Hand Polarization: If one's right hand thumb points in the direction of propagation and the fingers curl in the direction that $\vec{E}$ changes.

  Left-Hand Polarization: The one that is not Right-Hand polarization is Left-hand polarization. While figuring out the correct state of polarization, left hand should be inside the pocket. Always.

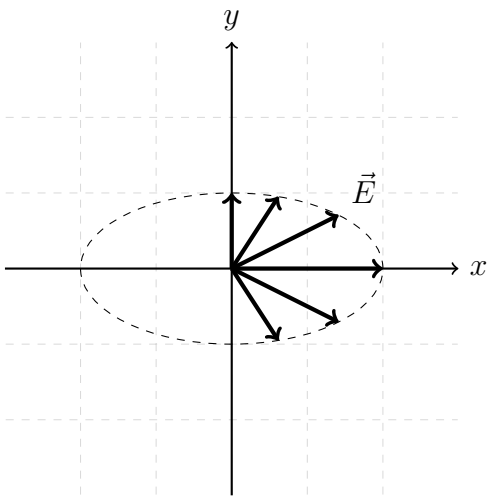

Figure 2.13: An illustration of the variation of electric field with time in the case of elliptical polarization in the $z = 0$ plane

- Circular Polarization is when the magnitude of the electric field vector $|\vec{E}|$ does not change with the change in direction in time. The major and the minor axis of the polarization ellipse are the same. This is a special case of elliptical polarization. A 3D view of a right-handed circularly polarized wave is shown in Figure 2.14. Similarly the left-handed version is shown in Figure 2.15. Both of them have the changing direction of the electric field vector shown in red. These are referred to as the standard circular polarization Handedness conventions.

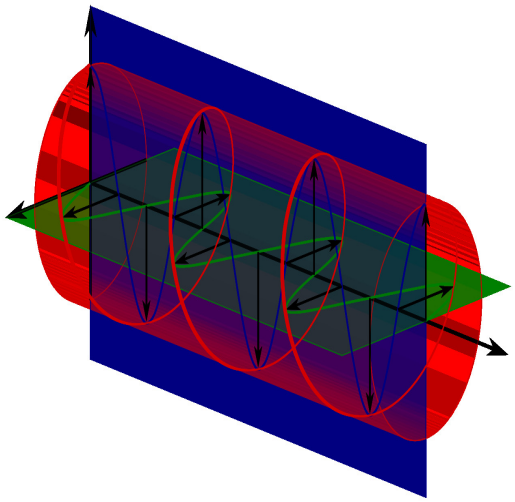

Figure 2.14: 3D view of a right-handed circularly polarized wave. Image courtesy: Wikipedia

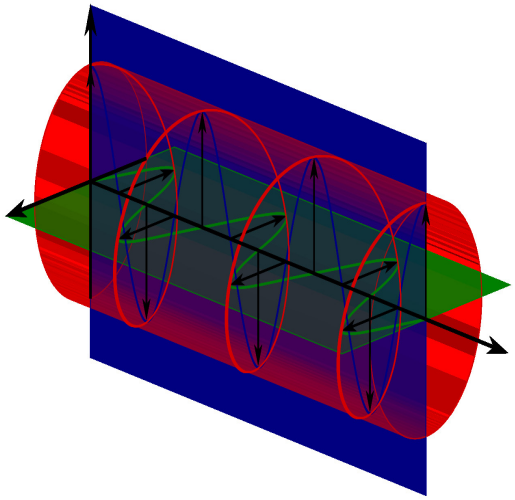

Figure 2.15: 3D view of a left-handed circularly polarized wave. Image courtesy: Wikipedia

Both the antennas discussed in this thesis are circularly polarized. The archimedean spirals are circularly polarized because of their basic shape. The patch antenna array can be made circularly polarized by arranging the patches in a specific way. More on this in section 3.3.

2.3.1 Axial Ratio

Axial ratio is an important parameter to describe quantitatively the amount of circular polarization of an antenna. The Axial Ratio (AR) is defined as the ratio between the minor and major axis of the polarization ellipse. Recall that if the ellipse has an equal minor and major axis it transforms into a circle, and we say that the antenna is circularly polarized. In that case the axial ratio is equal to unity (or 0 dB). The axial ratio of a linearly polarized antenna is infinitely big since one of the ellipse axis is equal to zero. For a circularly polarized antenna, the closer the axial ratio is to 0 dB, the better. Practically, antenna with AR less than $3dB$ is said to have circular polarization.

2.4 Theory on frequency independent antennas

This section is dedicated to the Rumsey's principle on frequency independent antennas [3] which describes in depth the fundamentals involved in making a physical structure extremely broadband. This section concludes with the equation of an Archimedean spiral antenna.

2.4.1 An opinion on frequency independence

Antennas are primarily resonant structures and in my personal opinion these antennas are not truly frequency independent. They can intuitively be assumed to have range of resonant structures at different operating frequencies all fused in a single profile. This statement may make more sense when a specific antenna in this class is discussed. After the idea and invention of frequency independent antennas, the engineers out of happiness, termed this extremely broadband nature as frequency independence. Such importance was given to these inventions. Of course, this is a hysterical take on the name.

A single parameter of an antenna spanning a frequency range of $10 : 1$ or higher is said to have frequency independence and the antenna works in that range. One needs

to elaborate here what "work" means since frequency independence is loosely defined. The antenna may have just a wideband input impedance match or an unaltered radiation pattern or polarization for that band of frequency of interest. Some parameter needs to operate over the $10:1$ bandwidth.

2.4.2 The General Equation for frequency independent antennas

For maximizing the bandwidth of an antenna it is experimentally found out that minimizing the finite lengths or abrupt edges and maximizing the angular dependence in the structure helps. Based on this conceptual understanding, one needs to make a few assumptions before stating that the antenna is frequency independent.

- The terminals of the antenna are vanishingly close to the origin
- There is symmetry about $\theta = 0^\circ$
- The antenna is infinitely extended
- The material is a Perfect Electric Conductor (PEC)
- The outline of the antenna is given by $\vec{r} = \vec{r}(\theta, \phi)$ where $\vec{r}$ is the distance vector to a given point on the antenna

Under these assumptions, a very generic approach is used to formulate a meaningful theory for the synthesis of a frequency independent antenna. For a given design at frequency f_1, if $r_1(\theta, \phi)$ is the appropriate design then at a lower frequency $f_2 = \frac{f_1}{K}$, $r_2(\theta, \phi)$ is appropriate. It is known that antenna structures become bigger as the operating frequency is lowered. So presumably, $r_2(\theta, \phi)$ must be bigger by the same scaling factor K. Hence,

$$r_2(\theta, \phi) = K \times r_1(\theta, \phi) \tag{2.15}$$

Since it is assumed that the antenna structure is infinite, any scaling done on it will be equivalent to rotation by some angle, say ϕ'. Hence,

$$r_2(\theta, \phi) = r_1(\theta, \phi + \phi') \tag{2.16}$$

For a frequency independent antenna, it should operate the same at both the frequencies f_1 and f_2. Essentially the antenna has not changed. It has just been rotated by some angle. One must find a function that can scale the frequency by rotating. Also, the first partial derivative of 2.16,

$$\begin{aligned} \frac{\partial}{\partial \phi'}\left(r_2(\theta, \phi)\right) &= \frac{\partial}{\partial \phi'}\left[K r_1(\theta, \phi)\right] \\ &= \frac{\partial K}{\partial \phi'} r_1(\theta, \phi) + \frac{\partial r_1(\theta, \phi)}{\partial \phi'} K \\ &= \frac{\partial}{\partial \phi'}\left[r_1(\theta, \phi + \phi')\right] \end{aligned} \tag{2.17}$$

Here, the value of K and ϕ' are related. For a specific value of scaling K, ϕ' denotes the amount of rotation the antenna undergoes. r_1 and ϕ' are not related.

$$\frac{\partial K}{\partial \phi'} r_1(\theta, \phi) = \frac{\partial r_1(\theta, \phi + \phi')}{\partial(\phi + \phi')} \underbrace{\frac{\partial(\phi + \phi')}{\partial \phi'}}_{=1} \tag{2.18}$$

Partial derivative of 2.16 with respect to ϕ,

$$\begin{aligned} \frac{\partial}{\partial \phi}\left[K r_1(\theta, \phi)\right] = K \frac{\partial r_1(\theta, \phi)}{\partial \phi} &= \frac{\partial}{\partial \phi}\left[r_1(\theta, \phi + \phi')\right] \\ &= \frac{\partial r_1(\theta, \phi + \phi')}{\partial(\phi + \phi')} \underbrace{\frac{\partial(\phi + \phi')}{\partial \phi}}_{=1} \end{aligned} \tag{2.19}$$

Comparing equations 2.18 and 2.19,

$$\frac{\partial K}{\partial \phi'} r_1(\theta\phi) = K \frac{\partial r_1(\theta, \phi)}{\partial \phi} \tag{2.20}$$

Multiplying both sides by $\frac{1}{Kr_1(\theta,\phi)}$

$$\underbrace{\frac{1}{K}\frac{\partial K}{\partial \phi'}}_{only\ depends\ on\ \phi'} = \underbrace{\frac{1}{r_1(\theta,\phi)}\frac{\partial r_1(\theta,\phi)}{\partial \phi}}_{only\ depends\ on\ \phi} \tag{2.21}$$

Let

$$a = \frac{1}{K}\frac{\partial K}{\partial \phi'} = \frac{1}{r_1(\theta,\phi)}\frac{\partial r_1(\theta,\phi)}{\partial \phi}$$

Hence,

$$\frac{\partial r_1(\theta,\phi)}{\partial \phi} - ar(\theta,\phi) = 0$$

This is a first order differential equation. The solution is obtained through the separation of variables method. Let $r_1(\theta,\phi) = f(\theta)g(\phi)$. This implies

$$\frac{dg(\phi)}{d\phi} - ag(\phi) = 0$$

'g' can satisfy this equation if $g(\phi) = e^{a\phi}$. Hence in an ideal case, for an antenna to be frequency independent the following mathematical conditions 2.22 and 2.23 need to be satisfied.

$$a = \frac{1}{K}\frac{\partial K}{\partial \phi} \tag{2.22}$$

$$r_1(\theta,\phi) = f(\theta)e^{a\phi} \tag{2.23}$$

It is important to recall that Equations 2.22 and 2.23 refer to ideal conditions where the antennas are assumed to be infinitely large and so on. Realistically this is not possible. Also, this a general form of the necessary conditions and the antenna shape must be an implementation of 2.23. The archimedean spiral, which is the focus for this text, is also a specific implementation of this equation.

2.5 Planar Equiangular Spiral

It will be apparent later in the text that the Archimedean Spiral is based on the planar equiangular spiral antenna. The planar equiangular spiral is governed by the following equation

$$\frac{df(\theta)}{d\theta} = A\delta\left(\frac{\pi}{2} - \theta\right) \tag{2.24}$$

where r, which is the radius to the actual wire ends up being the following value.

$$r = \begin{cases} r_0 e^{a(\phi-\phi_0)} & \text{if } \theta = \frac{\pi}{2}, \\ 0 & \text{else.} \end{cases}$$

$r = Ae^{a\phi}$ implies $\phi = \frac{1}{a} ln \frac{r}{A}$. Let $tan\,(\psi) = \frac{1}{a}$. This gives

$$\phi = tan\,(\psi)\,[ln(r) - ln(A)]$$

The bandwidth of the planar spiral depends on the length of the feed at the center and the overall radius of the spiral. Smaller feed dictates higher operating frequency while bigger radius makes the antenna operate over lower band.

The adjacent arms of the equiangular spiral have increasing distance between them as the structure grows. This analysis so far assumes that the width of the wire is infinitesimally small.

2.6 The Archimedean Spiral

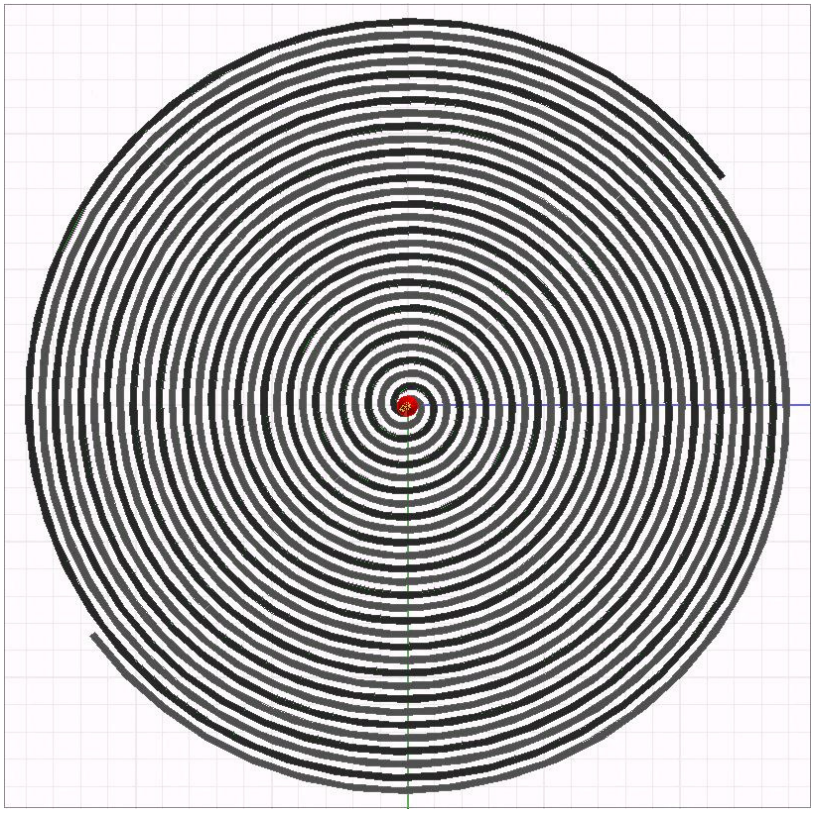

Figure 2.16: Top view of a conventional archimedean spiral design in HFSS

The archimedean spiral is essentially a simplified version of the equiangular spiral. Here, the distance between two adjacent arms remains constant unlike the equiangular spiral. The governing equations are an approximation to the equiangular spiral,

$$r = r_0\phi \tag{2.25}$$

If it is a two arm spiral, the other arm is rotated by 180° and the equation for the second arm is $r = r_0(\phi - \pi)$. This means that there are a lot more turns in the same amount of space. An example of a conventional two arm spiral with ten turns is shown in Figure 2.16.

2.6.1 An intuitive understanding

This approach is based on the working of a dipole antenna. Figure 2.17 shows a simple dipole antenna design. The structure of the Archimedean spiral antenna can be thought of as a collection of such dipoles of varying lengths twisted and stacked on the same plane. To better understand the previous statement, assume that a twisted dipole of some length corresponding to frequency f_1 exists, as shown in Figure 2.18 (a). Similarly there are other dipoles with different lengths resonant at frequencies f_2, f_3 and f_4. Here $f_1 > f_2 > f_3 > f_4$.

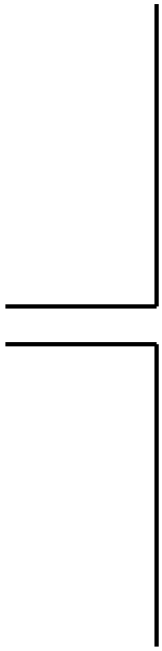

Figure 2.17: A simple dipole antenna design

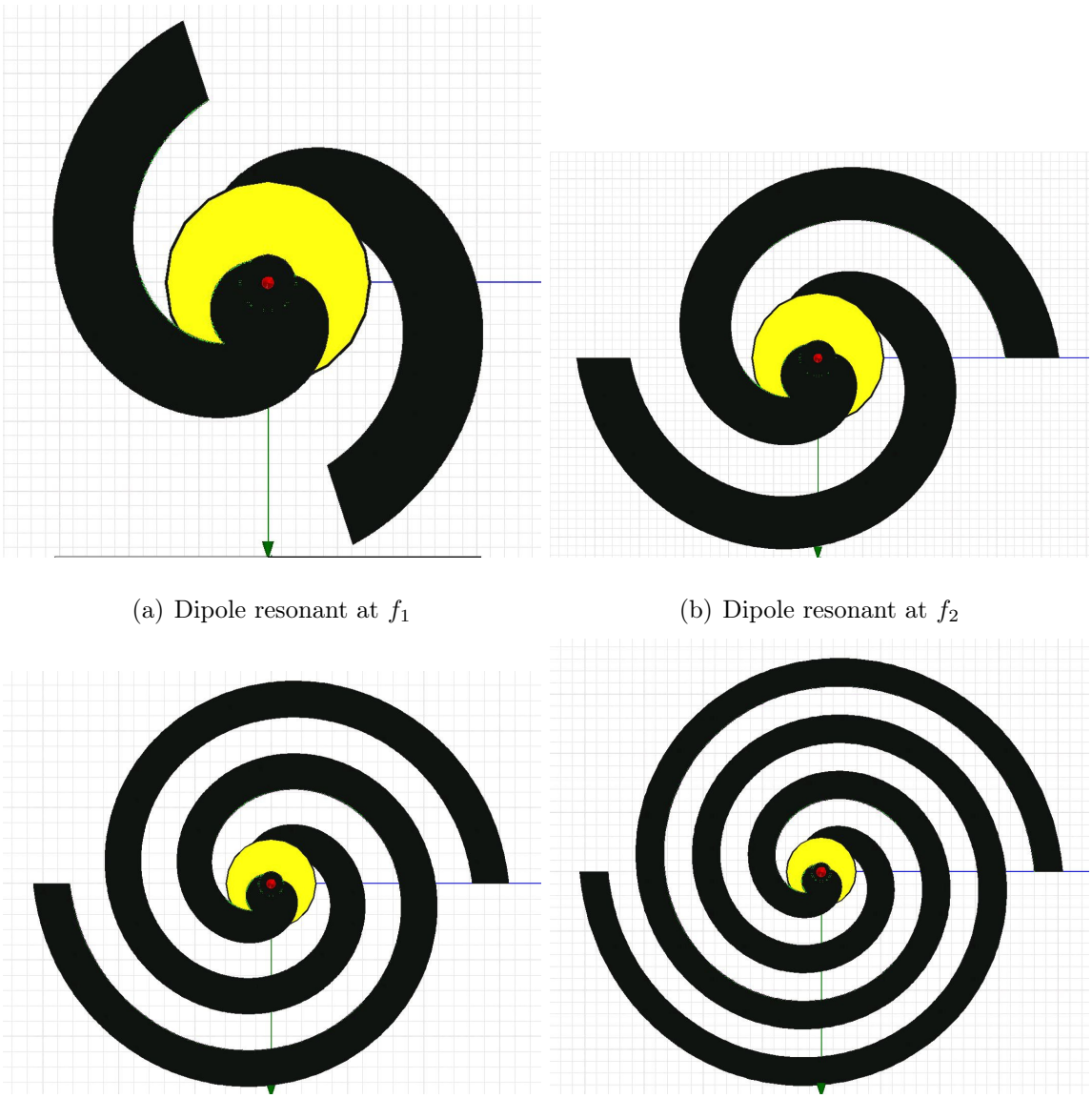

(a) Dipole resonant at f_1

(b) Dipole resonant at f_2

(c) Dipole resonant at f_3

(d) Dipole resonant at f_4

Figure 2.18: Twisted dipoles of varying lengths

The length of each dipole is now a function of the angle at which the spiral rotates. Since these dipoles with different resonant frequencies collectively constitute the spiral antenna, there can be infinite number of resonances in a specific band of frequencies. Depending on the input frequency, the corresponding length inside the structure radiates. This makes the spiral antenna radiate at all frequencies at which the dipoles resonate and hence makes it frequency independent.

CHAPTER 3: CIRCULARLY POLARIZED FOUR ELEMENT TWO PORT PATCH ANTENNA ARRAY

3.1 Application Background

Conventional patch antenna arrays have a single input port. If the signal entering through the port has the operating frequency of the patches, the power radiates away in free space through the patches. For all other frequencies except this resonant frequency, this power reflects back into the port. The top view of a model in ANSYS HFSS of such a conventional patch antenna array is shown in Figure 3.1. It is 4 element patch array with series offset microstrip feed.

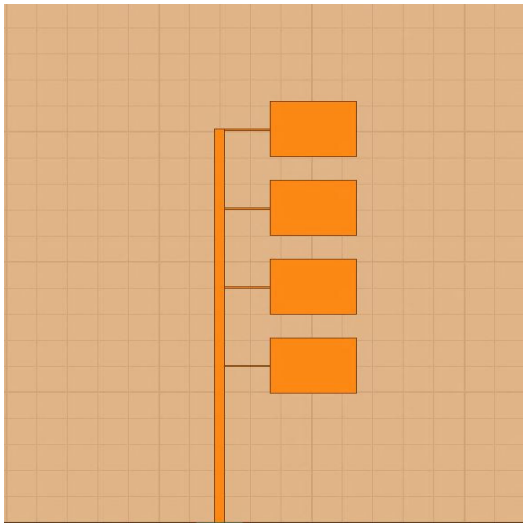

Figure 3.1: Top view of a four element patch array model constructed in Ansys HFSS.

Regarding the design of the circularly polarized patch array shown in Figure 3.2, there is an addition of one more port at the other end of the feed line and the structure in essence is a two port network. Power enters one port and leaves through the other port. If the input frequency is the operating frequency of the patches, that

power radiates away and minimum power is seen at the other port. For all the other frequencies except this resonant frequency, the signal flows from one port to the other through the 50Ω matched microstrip feed. This property is exploited further and elaborated in sections 3.1.1 and 3.1.2.

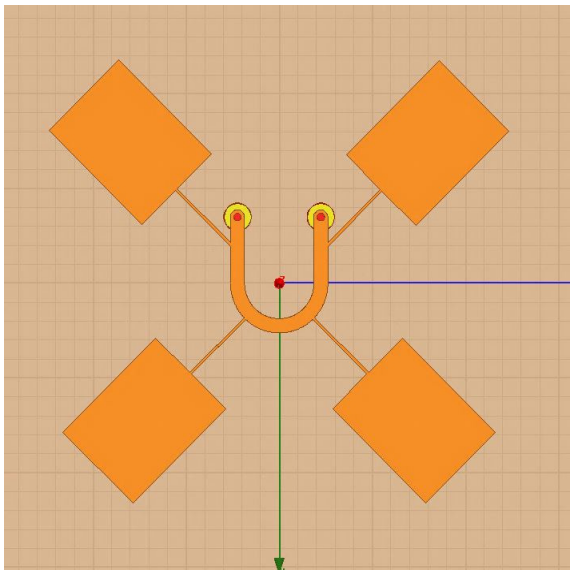

Figure 3.2: Top view of the final design of the circularly polarized four element patch antenna array model constructed in Ansys HFSS.

3.1.1 Encrypted Polarization

Since there are two ports, both of them can be used as input ports, but not simultaneously. If feeding the structure from one port gives a right-handed circular polarization, feeding it from the other port will change it to left-handed because of the symmetry and reversal. Switching the signal from one port to the other while match terminating the unused port will change the polarization of the radiated signal on the fly. The resultant radiation will have a right-handed and a left-handed polarization component. One can assume Figures 2.15 and 2.14 interleaved with one another at different intervals in time. Any conventional antenna, which will always have fixed polarization, will not be able to decipher this signal since a conventional antenna cannot "catch" the missing polarization component.

The switching frequency of the ports can be made higher than the operating fre-

quency of the patch antenna array. In this way, a single cycle of radiated data can have multiple polarizations. There is then only one way to receive such dual polarized signals. This communication scheme can only work when the transmitting and the receiving antenna are of the same kind and switching frequency of the ports is phase-synchronized. Without this synchronization too, the communication link will fail.

To summarize, the antennas on both the ends must be capable of changing the polarization of the radiated signal on the fly and the switching frequency of this "changing polarization" must be phase-synchronized. In essence, there is now a new layer of security added at the antenna end of a transceiver system which encrypts polarization. This can be particularly useful in military applications where one can have multiple such systems having the same operating frequency but different switching frequencies.

3.1.2 Radiative filters

As the microstrip antennas are based on the resonant cavity model, they are inherently narrow band. For most of the research community out there, this narrow band response is a challenge to overcome. For the purpose of this thesis, it is a welcomed advantage.

The two coaxial ports are connected via a microstrip line on the antenna. This antenna can be used as a stub on a continuous transmission line. At the resonant frequency of $5GHz$, signal fed through any of the ports will radiate away from the patches in free space. At all other frequencies, the signal will continue to transit from one port to the other on the transmission line and the antenna will not act as a stub. At $5GHz$ the power will be lost from the transmission line into free space.

The antenna is hence behaving as a narrow band notch filter at $5GHz$ and it is radiative in nature.

3.2 Antenna design specifications

The antenna consists of four rectangular patches arranged in a circular fashion. The design procedure involves calculating the length and width of the radiating element, the width of the quarter-wave transformer and the feed structure that connects the four patches. This section talks about their design in that specific order.

The design procedure for the patch involves assuming that the relative permittivity of the dielectric medium ϵ_r, the operating resonant frequency f_r and the height of the dielectric substrate are known. For the design under consideration $\epsilon_r = 4.4, f_r = 5GHz$ and $h = 0.79mm$.

1. The width W of the patch is calculated depending on the type of feed. For a microstrip feed, there is an optimal width given in open literature which is used here as a guide

$$W = \frac{1}{2f_r\sqrt{\mu_0\epsilon_0}}\sqrt{\frac{2}{\epsilon_r + 1}} \tag{3.1}$$

   With the input parameters given, the width turned out to be $10.5848mm$.

2. The effective dielectric is calculated based on the formula for a microstrip line as given in [15].

$$\epsilon_e = \frac{\epsilon_r + 1}{2} + \frac{\epsilon_r - 1}{2}\frac{1}{\sqrt{1 + 12\frac{h}{W}}} \tag{3.2}$$

   For the width of the patch element, $\epsilon_e = 3.93$

The patches are arranged in a circle and spaced a quarter wavelength λ_e apart to accommodate circular polarization. λ_e is the effective wavelength corresponding to the phase velocity obtained in the dielectric medium. The center of the radiating elements are distant by half of the free-space wavelength λ_0.

For feeding the patches, a 50Ω microstrip line and an offset series feed method is used. The ends of the feed are connected to coaxial connectors. Although the cables are thinner, the connectors are approximately $8mm$ in diameter. For the antenna feeding to be possible physically with these connectors, the end points of the circular feed must be at least $9mm$ apart, where $1mm$ is kept for tolerances. At $5GHz$, the physical distance between the patches of $\frac{\lambda_e}{4}$, is calculated to be $17.12mm$. For $9mm$ diameter of the coaxial connectors, $18mm$ is the minimum required distance. Hence practically, it is not possible to arrange the feed in a perfect circle and some trade off must be made in order to fabricate the antenna where it is feasible to connect the cables.

3.3 Antenna feed design options

Several feed methods were simulated in Ansys HFSS keeping in mind the design constraints of the antenna. The initial form of the antenna is shown in Figure 3.3 (a) while the finalized design is (g). Although, all these designs satisfied most of the design criteria, the hunt was for the one that went closest to these specifications. This section discusses about why the other feed designs did not work and why the final "U" feed was selected referring to the options shown in Figures 3.3 and 3.4.

- The First option was the microstrip feed shown in (a). The initial idea was to keep two switches on the antenna substrate and control them to direct the signal entering the microstrip feed left or right. The figure shows a simulation of the switch connected to the left. Since there was just one port, all the signal reflected back into the patches and adversely affected the gain.

- The switching very close to the radiating elements is bound to cause interferences. It was then decided to move the switching outside the antenna and use two ports instead of one emerging out as (b). This is where the antenna became

a two port network. Since the ports were very close to the first patch and the last patch, impedance match was an issue. It was suspected that signal did not get enough room to convert itself from the coaxial mode to microstrip mode. Also, ground plane was missing near connectors which would have affected the impedance at the input of the patches.

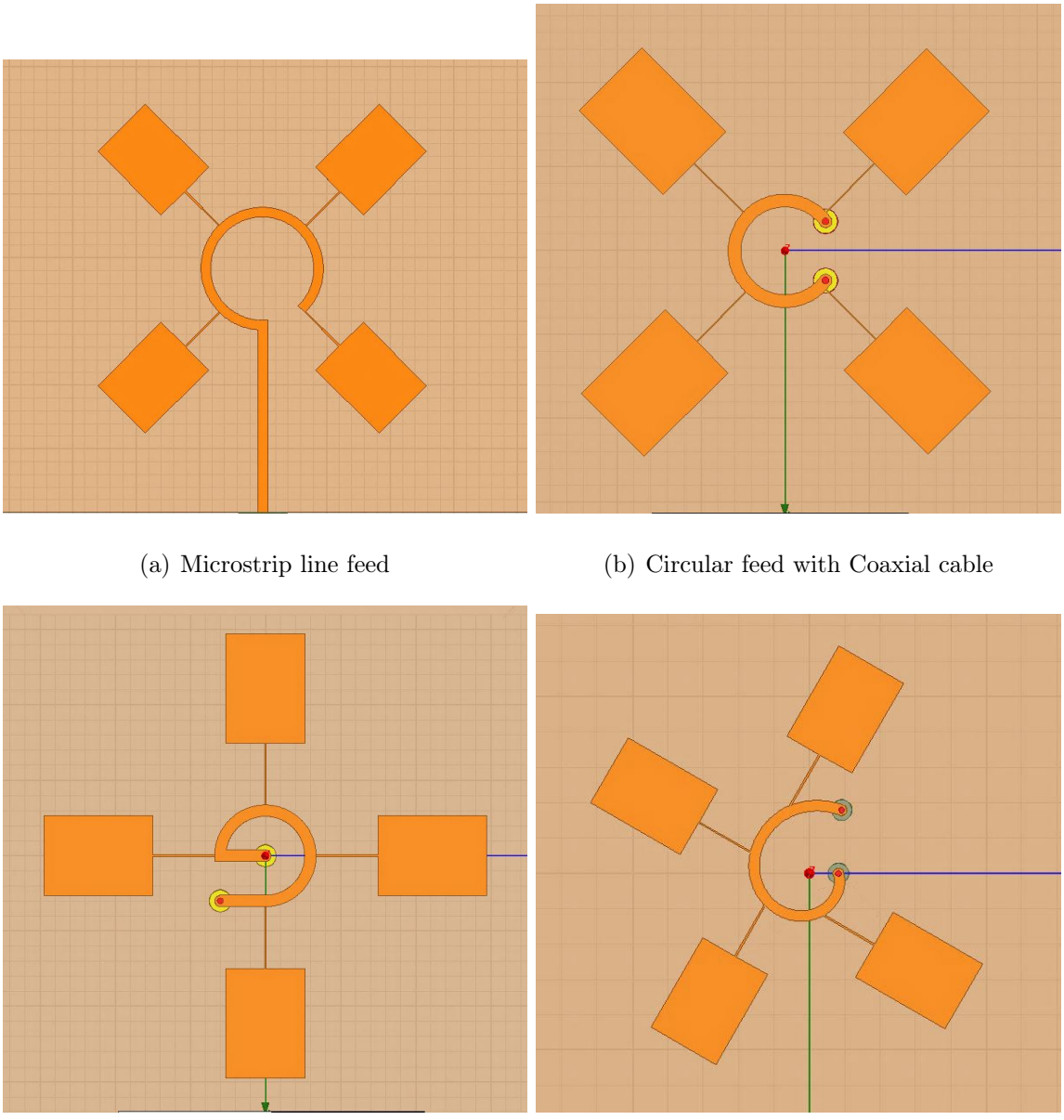

(a) Microstrip line feed

(b) Circular feed with Coaxial cable

(c) Circular feed with offset in coaxial ports

(d) Spiral feed

Figure 3.3: Top views of first four antenna feed options simulated in Ansys HFSS

- The ports were then moved away from the patches and from each other in (c). The only problem faced by this model was the reflection occurring near the sharp bend.

- This gave rise to the spiral feed option in (d). Although this solved all the problems from the previous models and achieved the highest gain of $4.389dB$, the radiation pattern was more elliptical than circular. The centers of the radiating elements were not equidistant from each other anymore.

- The feed shape was changed back to a circle and an attempt was made to move the ports away from each other in (e). The problem with this model is the turning radius. As per literature the radius of the bend must be at least four times the width of the trace to minimize losses. [16]

- The U bend radius was adjusted to meet the requirements in (f). Now since the radius was increased by a fraction of approximately $0.5mm$, the patches were no longer $\frac{\lambda_e}{4}$ apart. This additional phase difference decreased the gain by approximately $1dB$.

- The final idea was to create a circular feed with a radius that keeps the patches $\frac{\lambda_e}{4}$ apart and then extend the feed straight up to make a "U" as shown in (g). From a logical standpoint, it is expected to have a hint of elliptical polarization since the patches are not equidistant. Simulation data shows that this effect is minimum and the pattern is still circularly polarized.

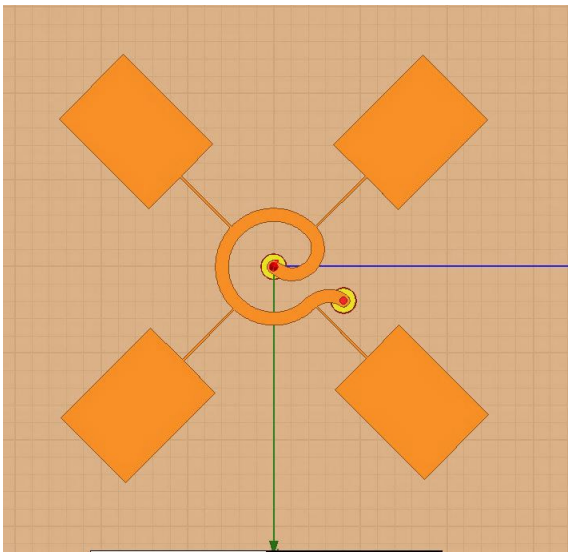

(e) The snake feed

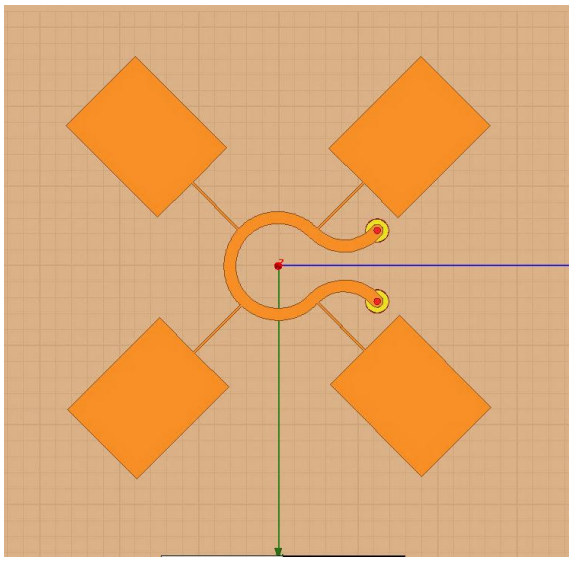

(f) The Ω feed

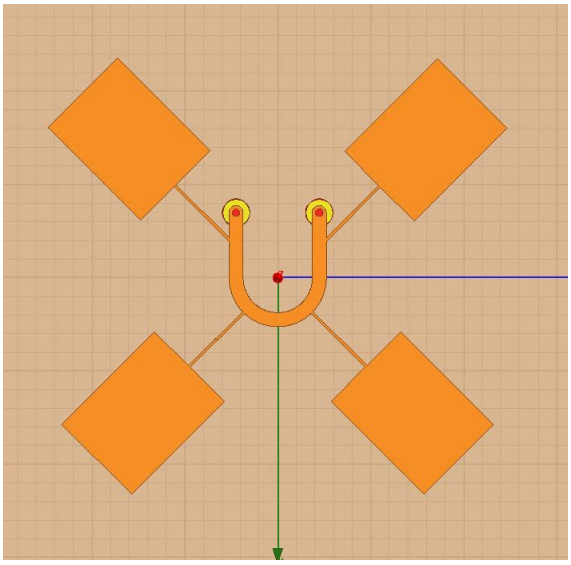

(g) The "U" feed

Figure 3.4: Top views of remaining antenna feed options simulated in Ansys HFSS

3.4 Simulation design and results

The simulations for all of the designs are done in Ansys HFSS (High Frequency Structure Simulator). For the two coaxial connections to the antenna, wave ports are used in HFSS and the coaxial cables are directly attached to the antenna instead of using a coaxial connector. Several other simulation environment settings are in

effect to give plausible results. For example, the air box is kept $\frac{\lambda_0}{4}$ away from the substrate to capture all the field variations. A mesh operation on the air box is also implemented to restrict the finite element length to $\frac{\lambda_0}{6}$. Here λ_0 is the free space operating wavelength corresponding to $5GHz$.

Regarding the simulation design, the complete antenna along with the substrate measures $70mm \times 70mm$. The width of the microstrip feed line is $1.5132mm$ to keep it at 50Ω. The quarter wave transformer attaching the feed and the antenna has a width of 0.2563 and has a length of $8.348mm$ which is equal to $\frac{\lambda_e}{4}$. The final length of the patch is $14.098mm$ while the width turned out to be $10.58mm$. The Ufeed curve radius is kept to be $5.233mm$ in order to maintain the four patch elements $\frac{\lambda_e}{4}$ apart. An FR-4 substrate of height $0.8mm$ and dielectric constant of 4.4 is used.

The simulated S_{12} and S_{21} for the U-feed design is shown in Figure 3.5. Both the values are identical with $-19.07dB$ at $5GHz$. The lowest is $-21.12dB$ at $4.98GHz$.

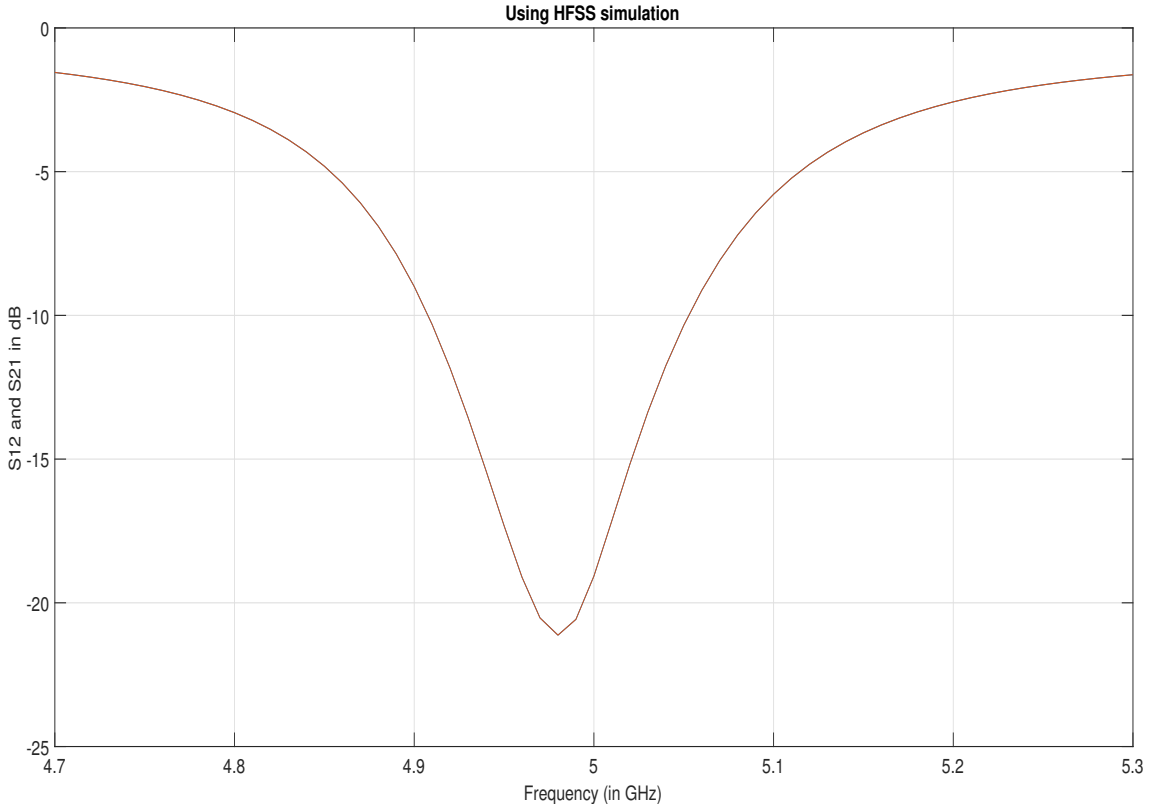

Figure 3.5: Simulated S_{12} and S_{21} in HFSS

Similarly, S_{11} and S_{22} are shown in Figure 3.6 where the plots are close to identical. S_{11} is $-12.47dB$ at $5GHz$. It is important to note that for a conventional one port antenna, one would see the curves reversed. Usually at the operating frequency, S_{11} would tend to fall down and stay at minimum to demonstrate lowest reflection. Most of the energy is radiated away at that frequency and the least is reflected back. For this antenna design, since the two ports are connected to coaxial cables through a 50Ω microstrip transmission line, the losses will be the least for all other frequencies except the operating frequency.

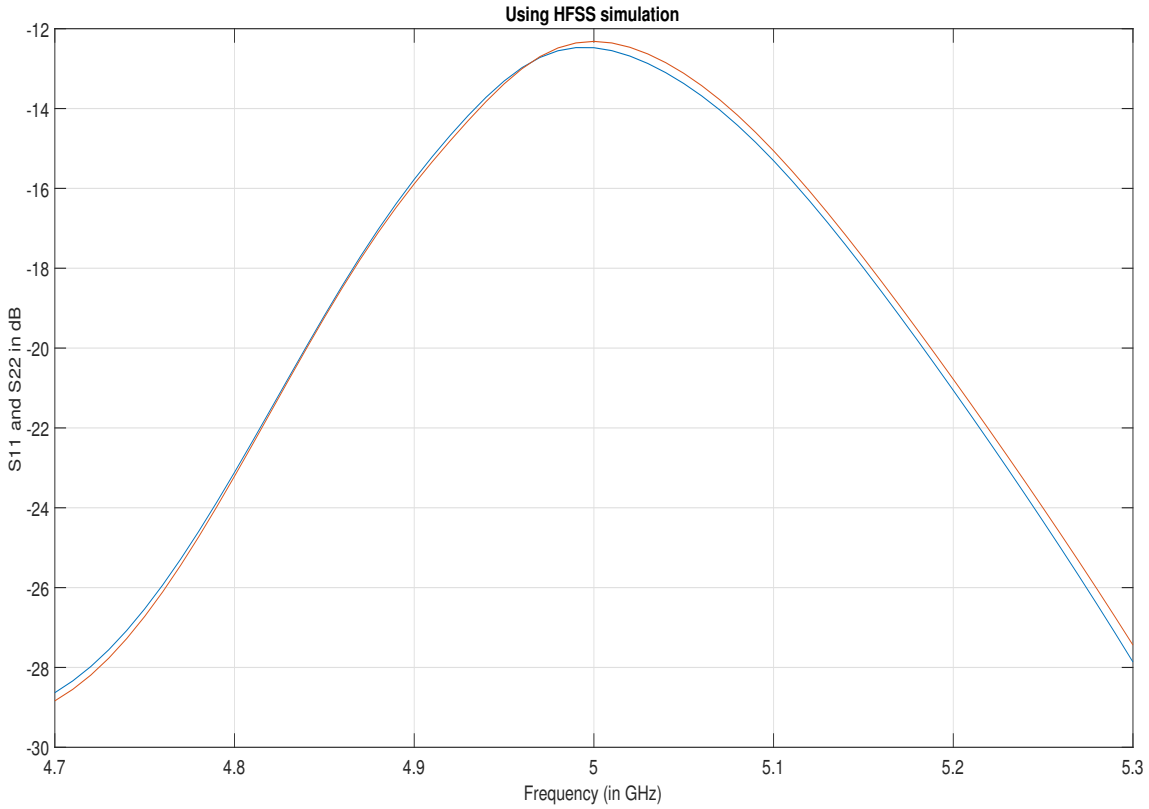

Figure 3.6: Simulated S_{11} and S_{22} in HFSS

The antenna is perfectly impedance matched in the band of frequencies up to which the coaxial cable is 50Ω but it does not radiate at all frequencies. Only at the resonant frequency of operation of the antenna, the S_{11} rises up to reach that value of reflection the structure provides and the energy is radiated out. Similar explanation

can be given for S_{12}.

The Gain pattern of the antenna in dB at $5GHz$ is shown in Figure 3.7. This is simulated using the port on the left of Figure 3.2 as input. The gain is $4.21dB$ at the center of the structure. As it can be seen, the pattern is circular, as expected, due to the geometry of the structure. Constructive contribution from every patch in enhancing the gain is also evident.

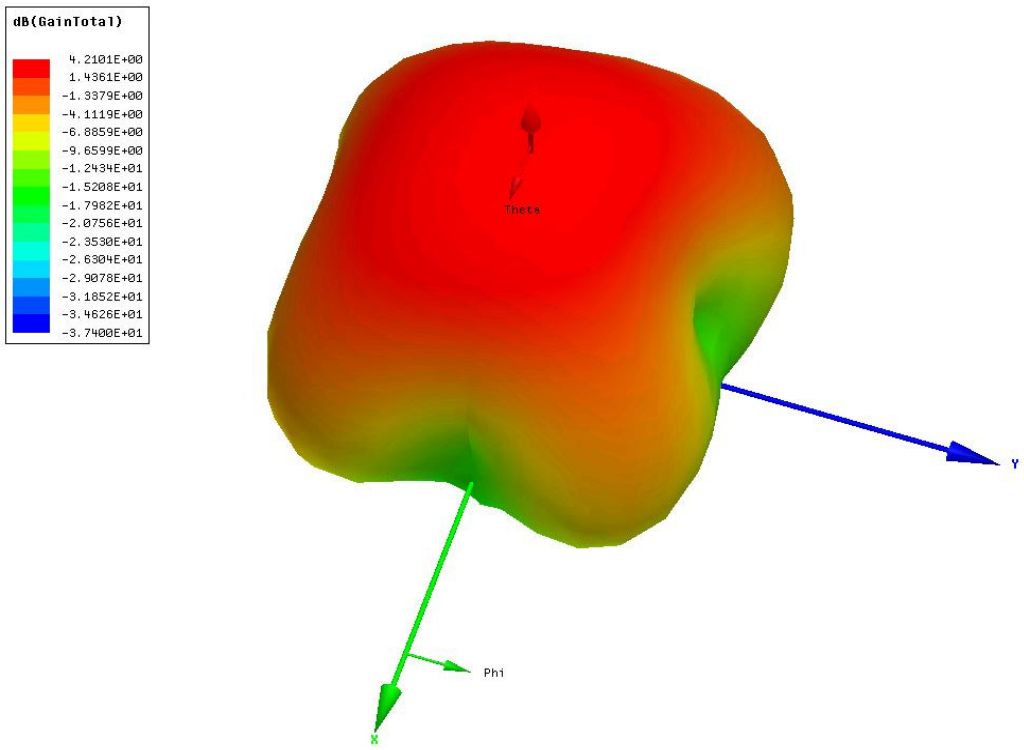

Figure 3.7: Simulated 3D gain pattern of the patch antenna array using the first port as input

The isolated gain patterns for the left-hand circular polarization and the right-hand circular polarization are shown in Figures 3.8 and 3.9 respectively. For the left-hand circularly polarized radiation, the gain is $-4.25dB$ while the right-handed circularly polarized radiation shows a gain of $4.139dB$. The input is fed from the left port in Figure 3.2 and the energy traverses the path from left to right, following the finger of

a folded right hand. So the polarization will be right-handed as is also evident from the gain pattern.

Changing the input port to the one on the right of Figure 3.2, one quickly gets the implications that the radiated wave will be left-handed circularly polarized. The energy then traverses clockwise in the structure opposing the direction of fingers in a folded right hand. Simulated evidence is shown in Figures 3.10 and 3.11. Right-hand circularly polarized wave has a gain of $4.15dB$ while the left-handed circularly polarized wave is down to $-4.26dB$.

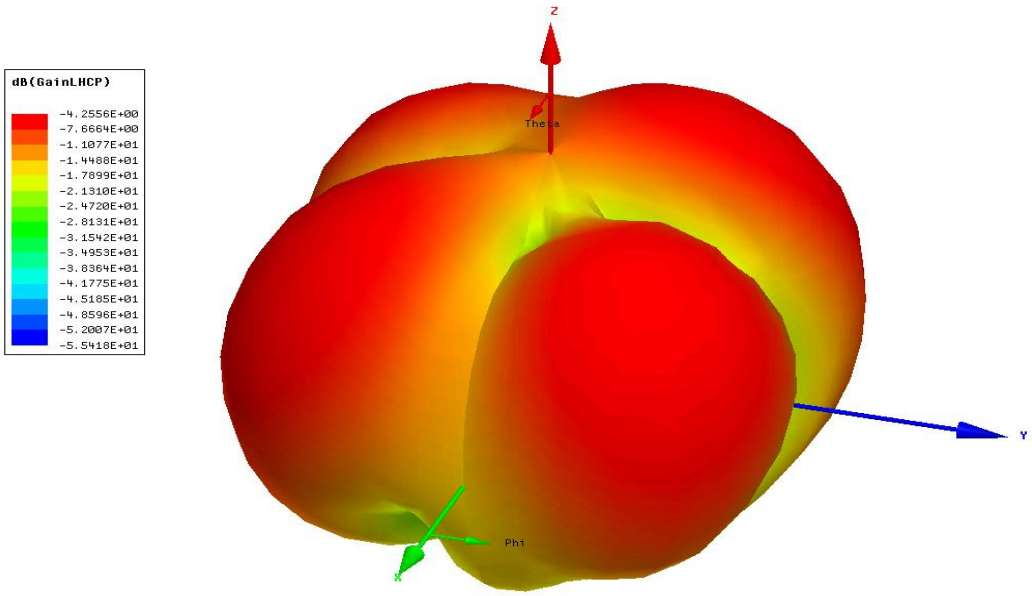

Figure 3.8: Gain pattern of the left-handed circularly polarized radiation

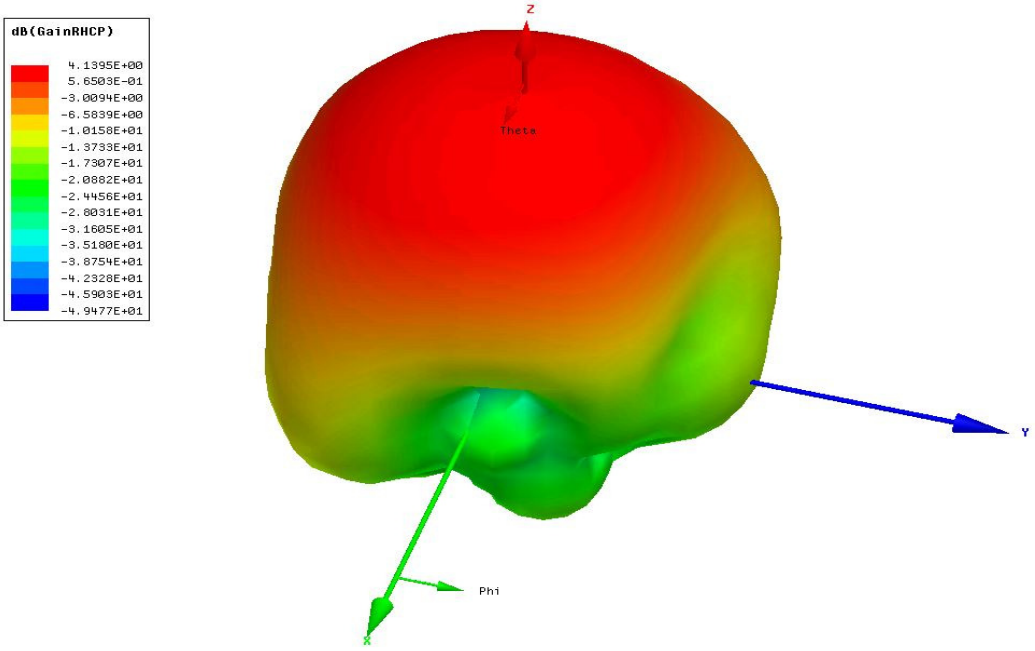

Figure 3.9: Gain pattern of the right-handed circularly polarized radiation with the left hand side port of Figure 3.2 as input

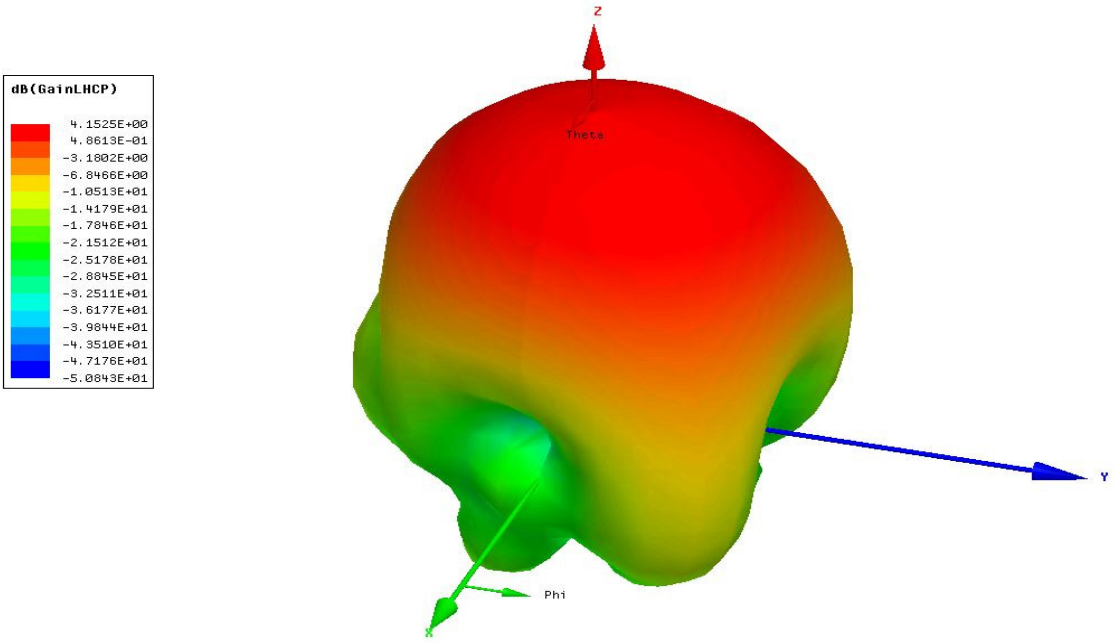

Figure 3.10: Gain pattern of the left-handed circularly polarized radiation with the left hand port of Figure 3.2 as input

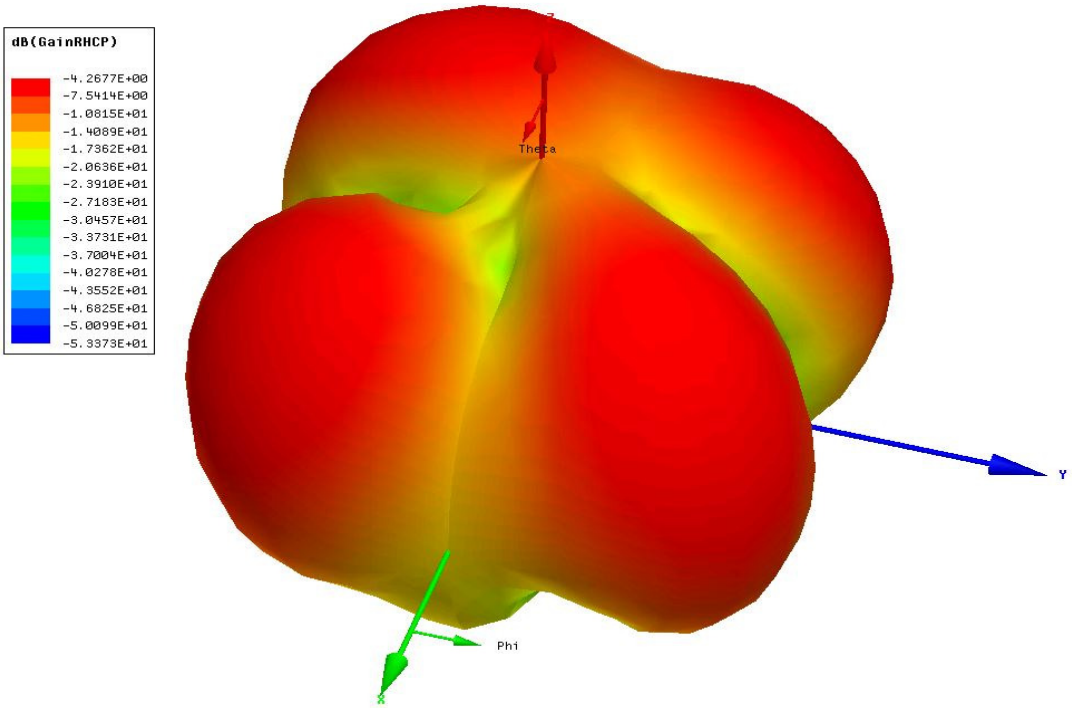

Figure 3.11: Gain pattern of the right-handed circularly polarized radiation with the right hand side port of Figure 3.2 as input

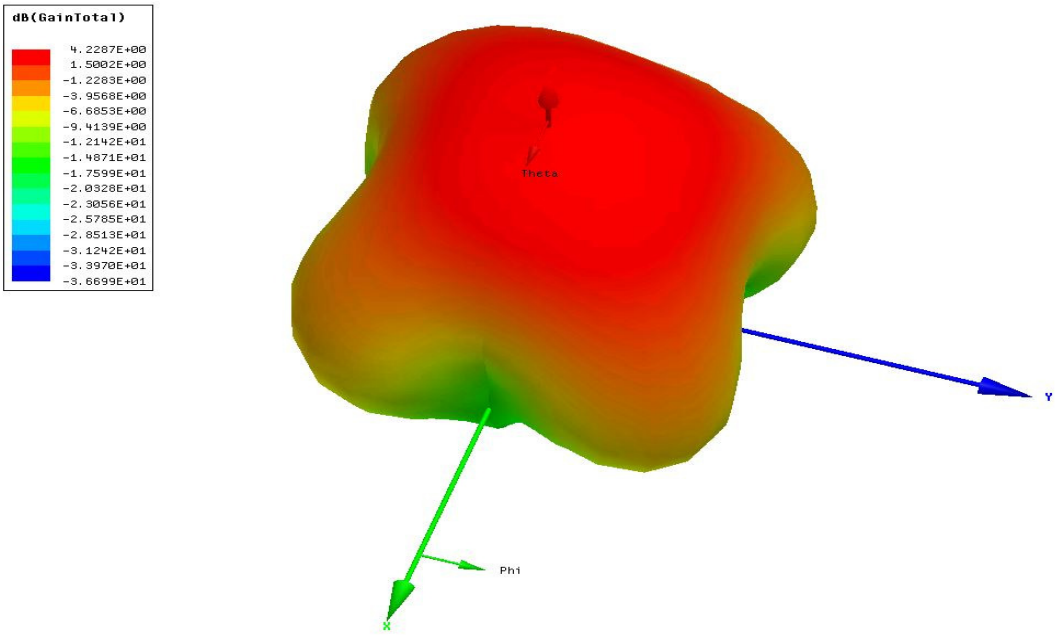

Figure 3.12: Simulated 3D gain pattern of the patch antenna array using the right hand side port of Figure 3.2 as input

Symmetry is also observed between both the ports in the design when the total gain pattern is observed. As shown in Figure 3.12, the maximum value of gain is at the center of the structure at $4.228dB$, which is very close to the value obtained for the other port as input.

The input impedance remains unaltered and is shown in Figure 3.13. It is $72.8 - j20.18\Omega$ at $5GHz$.

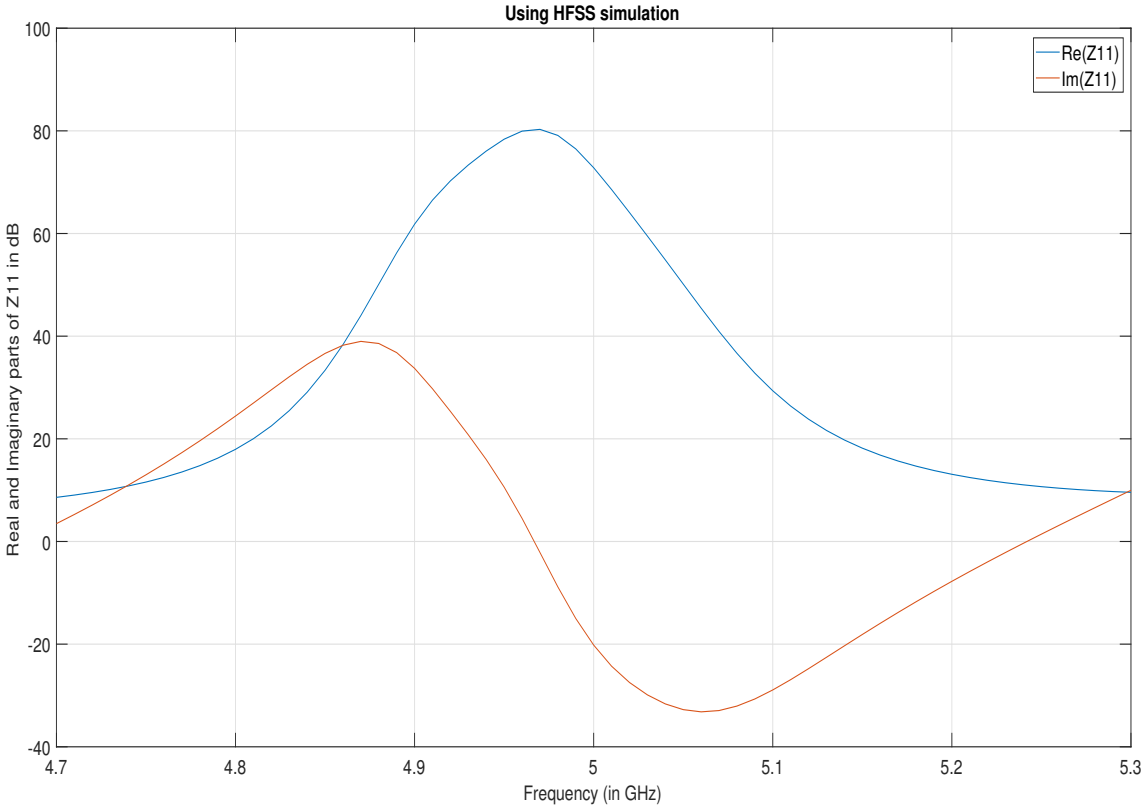

Figure 3.13: Simulated Z_{11} in HFSS

The structure emits circular polarization at the operating frequency. This is evident from Figure 3.14. The plot is for both the ports, not used simultaneously. As seen in the Figure, the axial ratio is less then $3dB$ in the vicinity of $5GHz$. This is the only region where the antenna radiates.

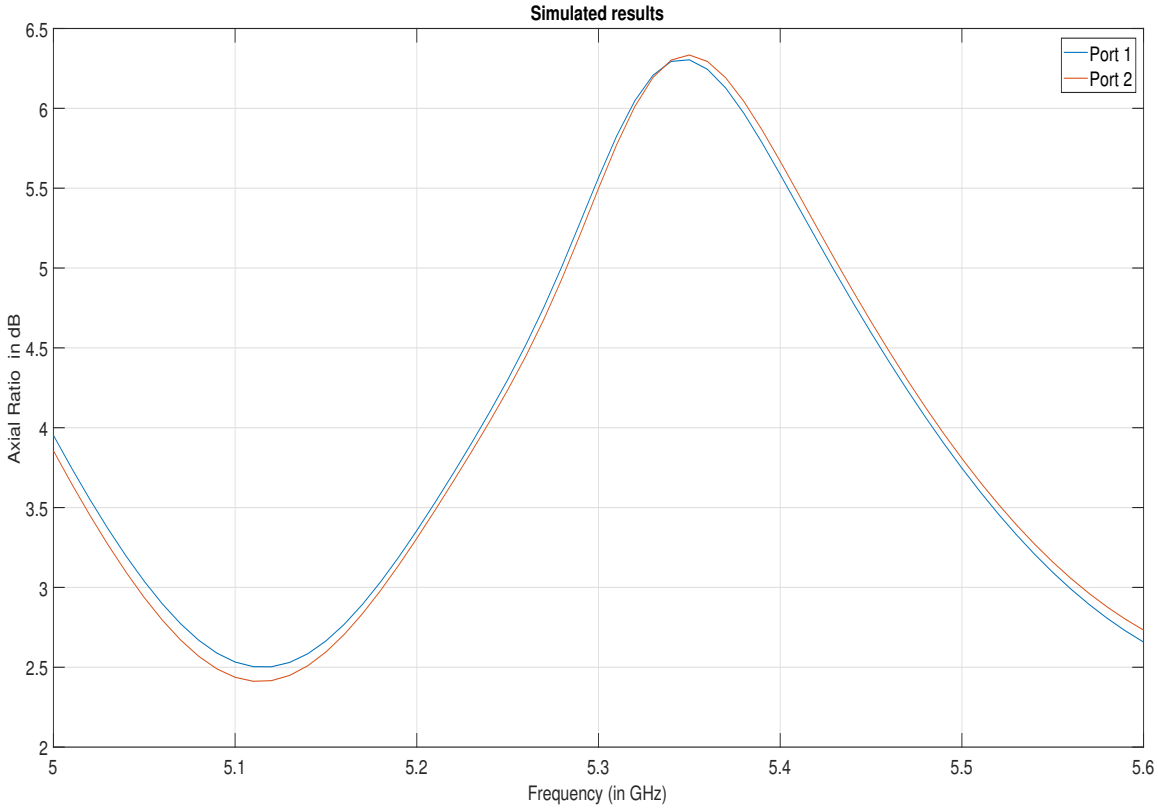

Figure 3.14: Axial Ratio in dB with respect to frequency for the U feed patch antenna array

The fact that the individual patches are at 90° phase apart, means that the energy adds up in time till it completes the full 360° circle along the U shape. One can observe different phases of the surface current densities on the structure in HFSS. This is shown through figures 3.15 to 3.18. The patches on the opposite corners have similar current densities while the adjacent patches differ in their pattern by 90°. As it was pointed out before in theory, this is a basic condition for circular polarization to occur efficiently. Not keeping the patches at the right distance might also give circular polarization to some extent but it will affect the axial ratio and the gain adversely.

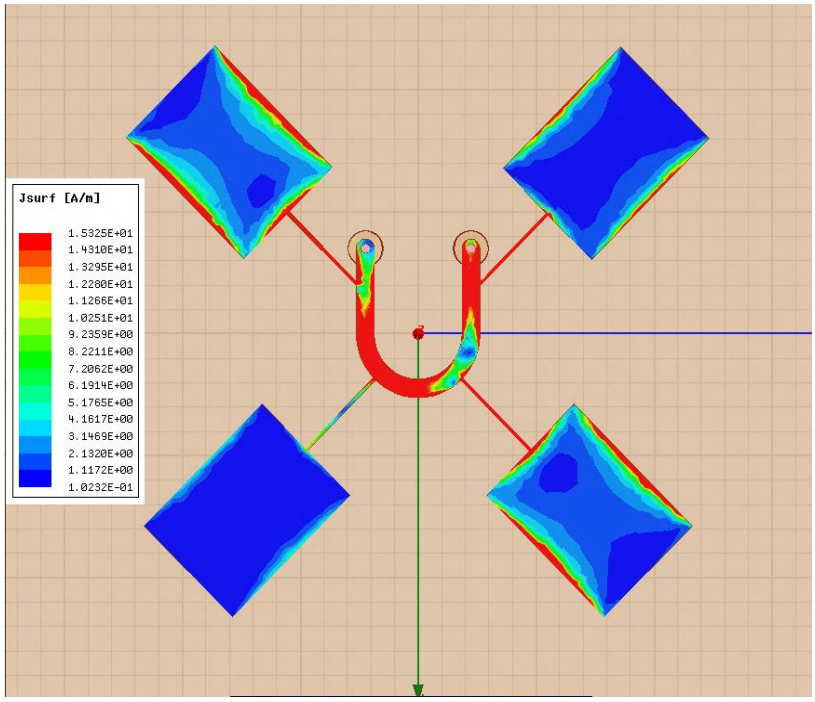

Figure 3.15: Surface current density on the U feed patch antenna array at 0° input phase of the signal

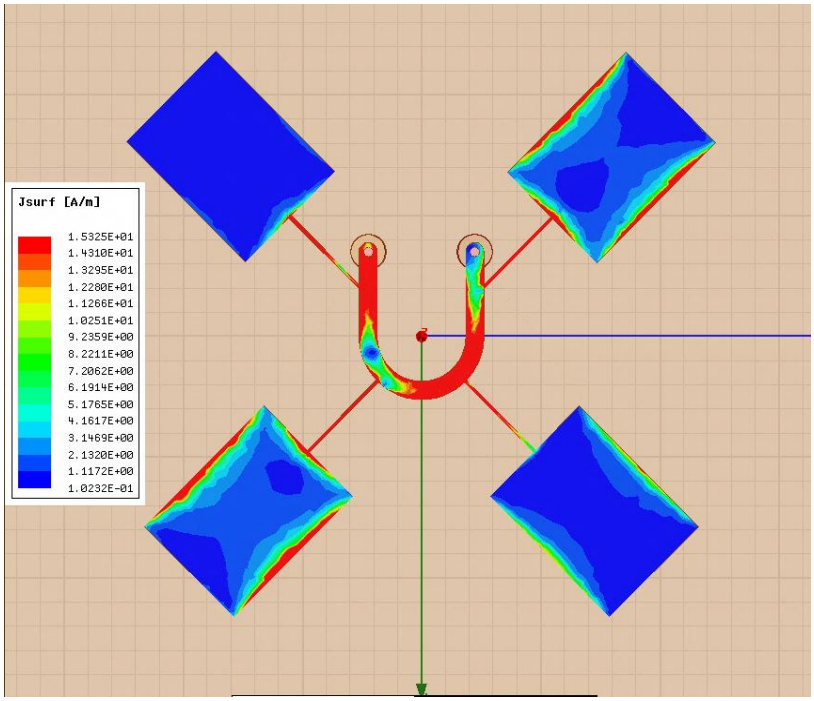

Figure 3.16: Surface current density on the U feed patch antenna array at 90° input phase of the signal

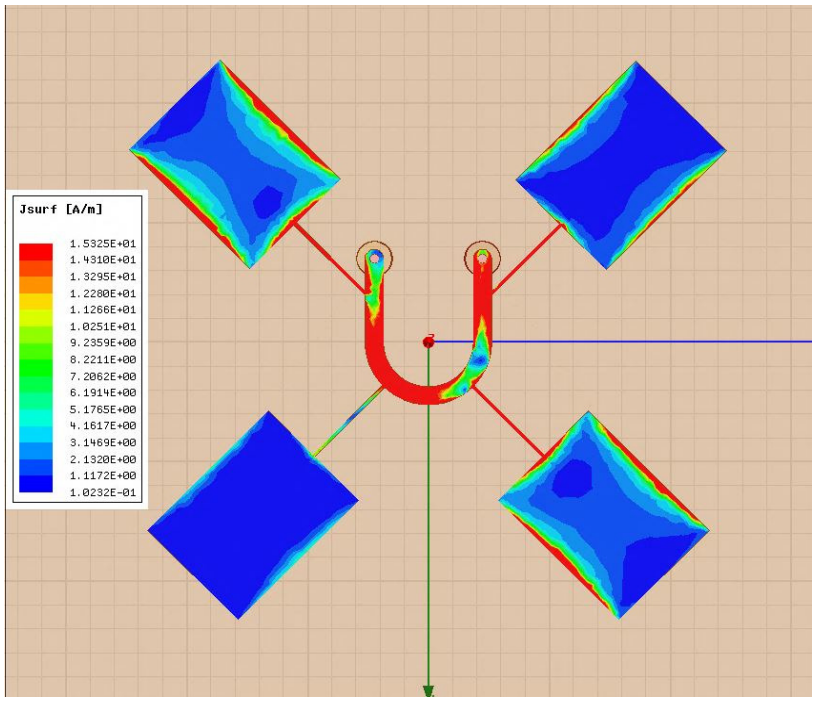

Figure 3.17: Surface current density on the U feed patch antenna array at 180° input phase of the signal

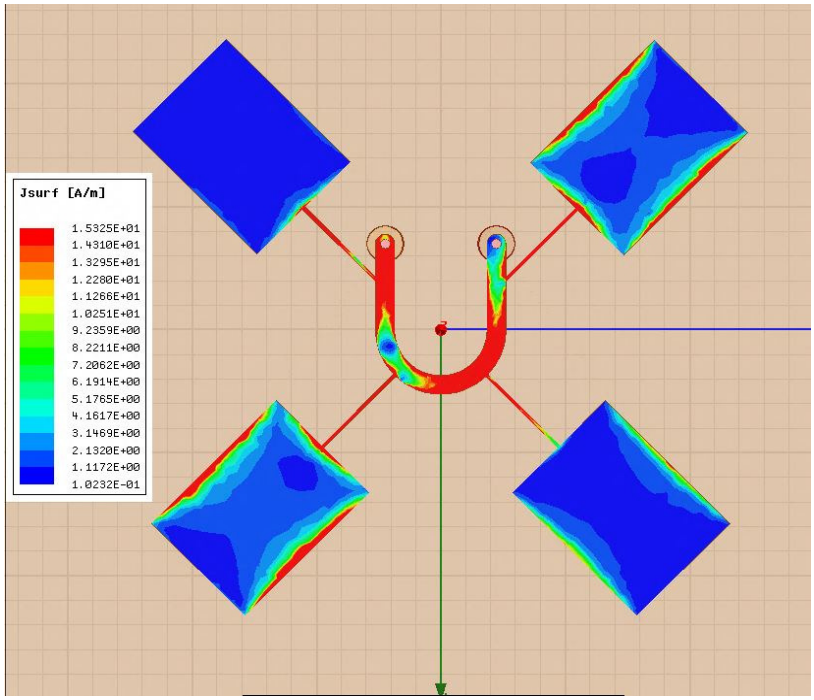

Figure 3.18: Surface current density on the U feed patch antenna array at 270° input phase of the signal

3.5 Measured data

Small tolerances can make a huge difference for narrow band structures. This was said by Dr. Adams from his experience in one of his lectures on Antennas. He is right indeed. The fabricated antenna design is shown in Figure 3.19.

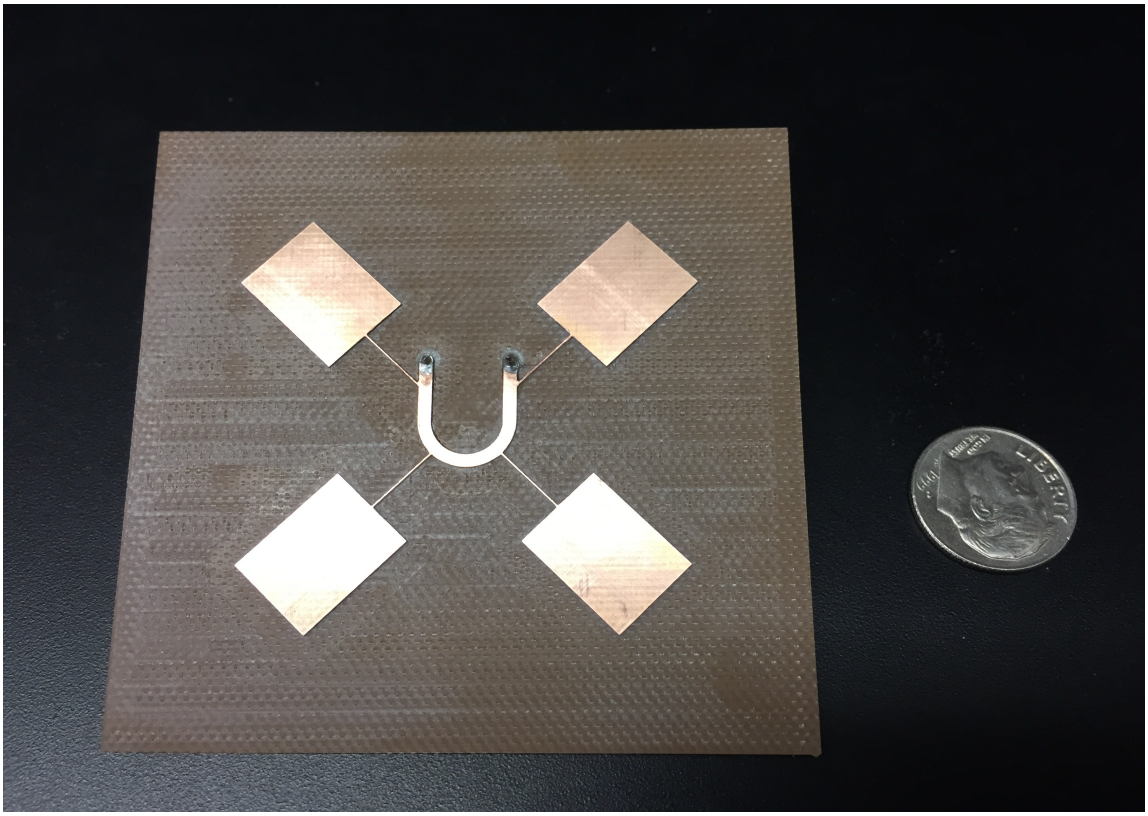

Figure 3.19: Fabricated four element patch antenna array

The measurements for this antenna were done on a two port Anritsu Shockline Vector Network Analyzer. The plot for S_{11} and S_{22} is shown in Figure 3.20 while the plot for S_{12} and S_{21} is shown in Figure 3.21.

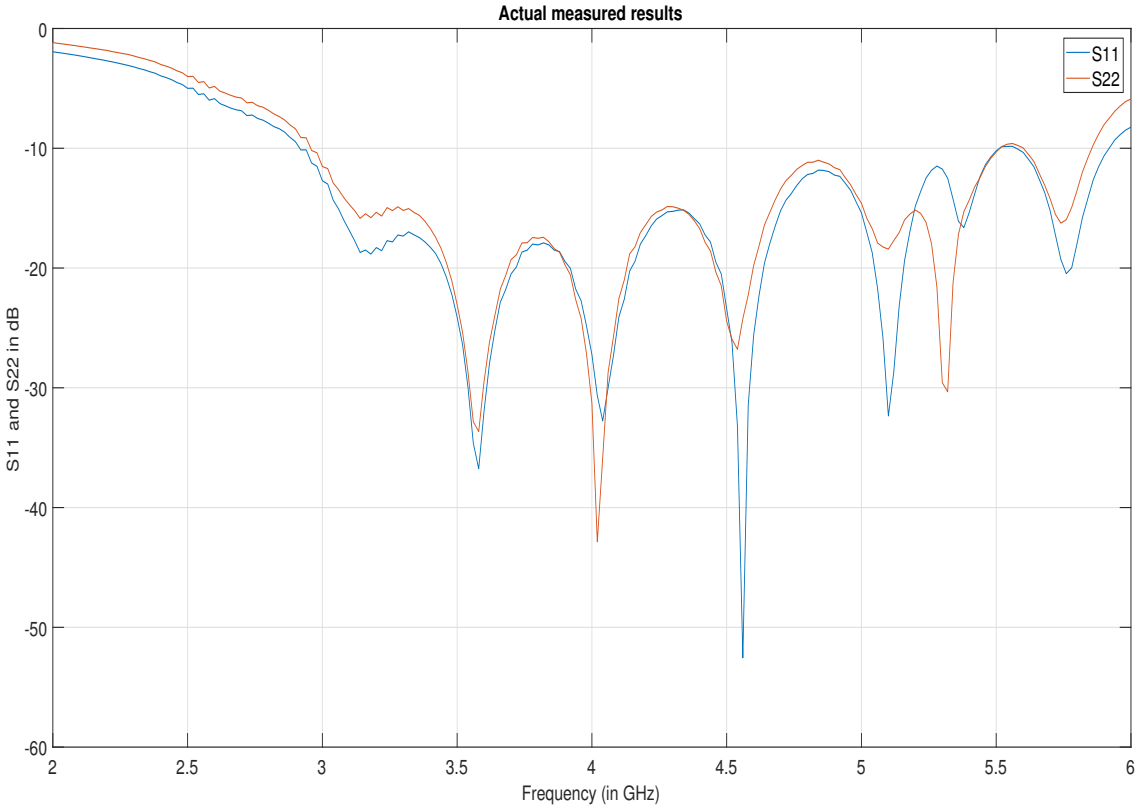

Figure 3.20: Measured S_{11} and S_{22} in dB of the patch antenna array

Even though there are multiple frequencies at which the antenna gives the least reflection, S_{12} makes it clear that the antenna radiates only at $5.31GHz$. This is the point where a dip is seen in the S_{12} curve. Note that the resonant frequency of operation is approximately $5.3GHz$ instead of $5GHz$. This shift in resonance can be due to various factors, primary being the substrate parameters. If the thickness of the substrate is different than the one used in simulation, the effective dielectric constant will change, shifting the frequency as per equation 2.8.

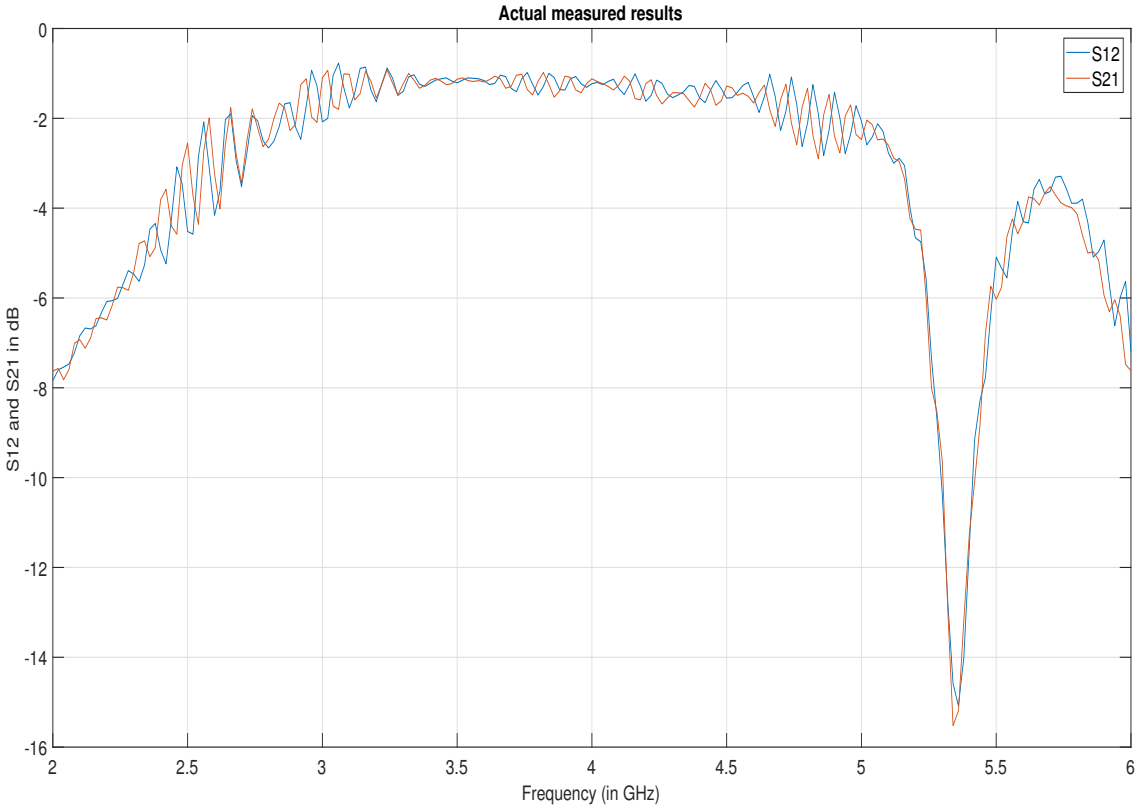

Figure 3.21: Measured S_{12} and S_{21} in dB of the patch antenna array

In order to substantiate for these results, an effective dielectric constant is calculated using $5.31GHz$ as the resonant frequency. The new value for dielectric constant turned out to be 3.82. In HFSS, the dielectric constant of the FR-4 material is changed to 3.82 instead of the default value of 4.4 and the antenna is simulated again. The results for the S-parameters after this amendment is shown in Figures 3.22 and 3.23. The resonant frequency did change as expected and the antenna now resonated at $5.3GHz$ matching with the actual results. The input impedance plot after the amendment is shown in Figure 3.24 as reference to exhibit the shift in resonance.

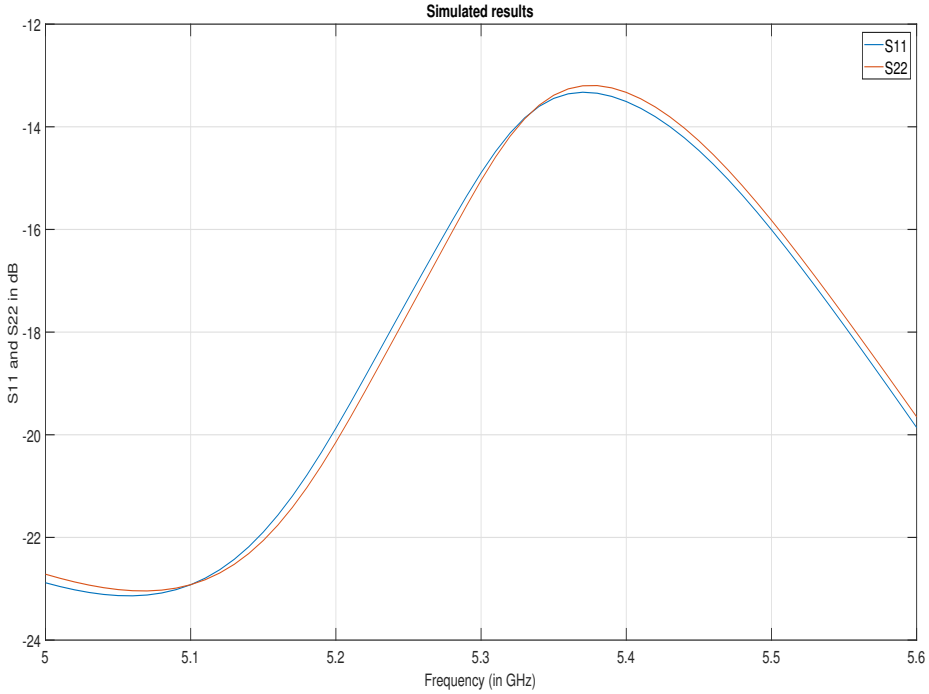

Figure 3.22: Simulated S_{11} and S_{22} in HFSS after changing ϵ_r to 3.82

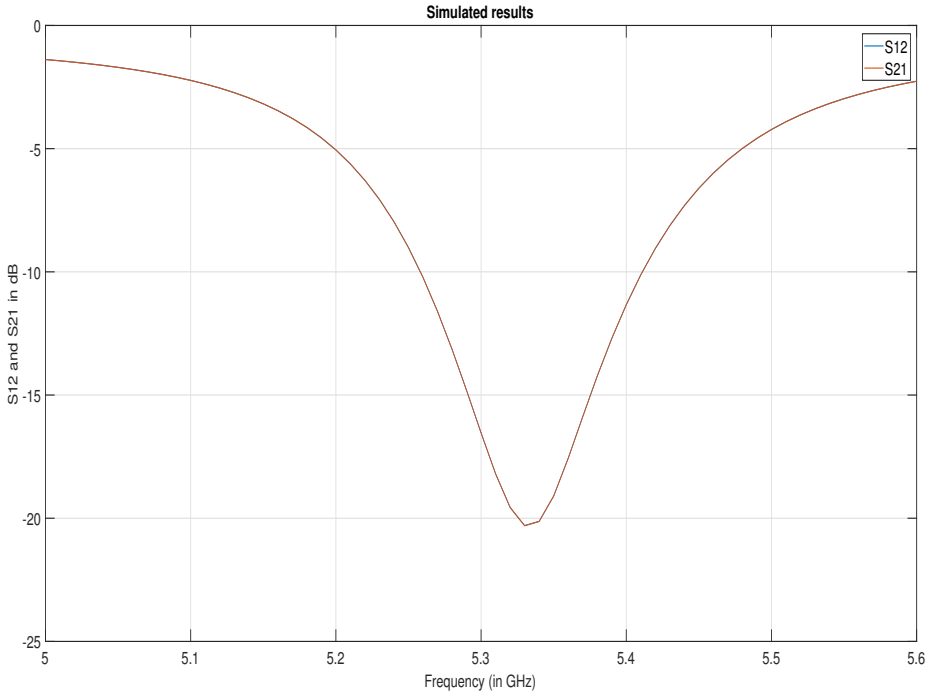

Figure 3.23: Simulated S_{12} and S_{21} in HFSS after changing ϵ_r to 3.82

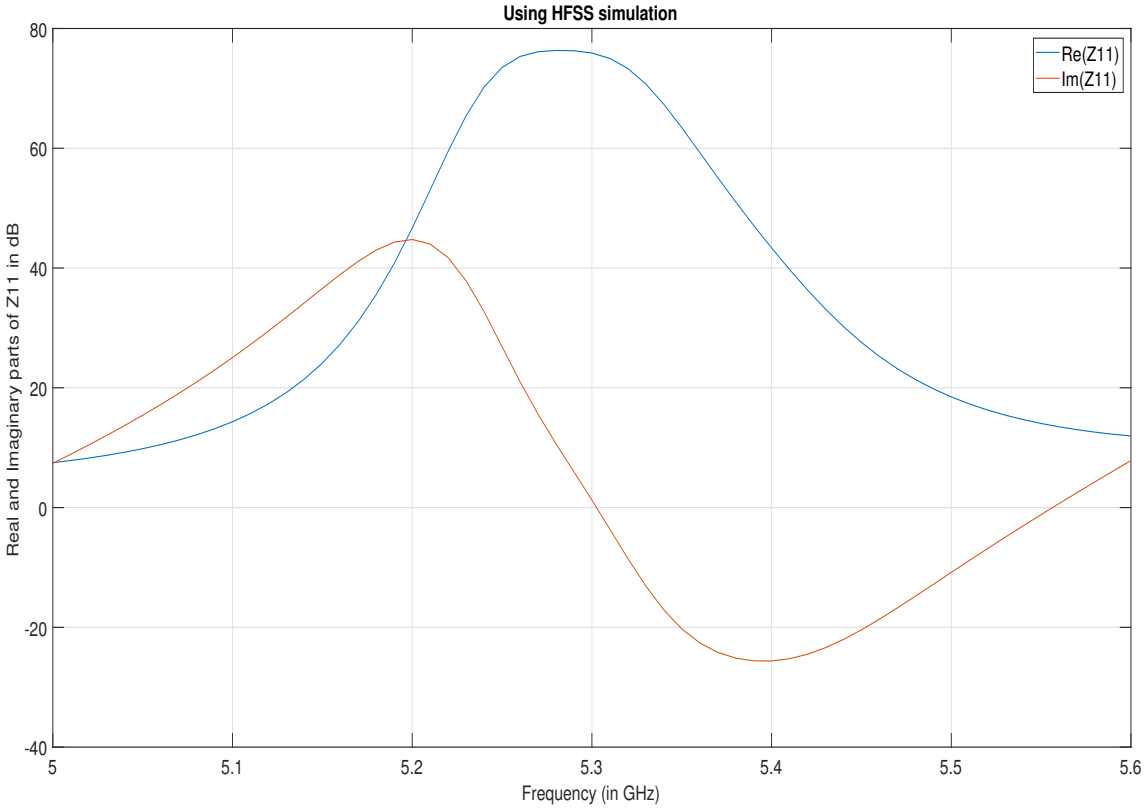

Figure 3.24: Simulated Z_{11} in HFSS after changing ϵ_r to 3.82

3.6 Conclusion

Making an antenna a two-port network can open an array of applications where it can be viewed as a filter element. It no longer have to be at the beginning or at the end of a transceiver. Changing the feed of the patch array gave a circularly polarized radiation pattern with minimal effect on gain. Compared to a straight offset series feed, the new design also saved board space and made the antenna compact.

CHAPTER 4: SELF-MATCHED 40:1 ARCHIMEDEAN SPIRAL ANTENNA

A noteworthy modification of the Archimedean spiral discussed in section 2.6 is explained here. The term "self-matched" refers to the fact that the antenna by itself does not need any mechanism or apparatus to match its input impedance to a 50Ω feed. The antenna structure inherently exhibits a 50Ω impedance at the feed point.

4.1 Applications

The goal of creating a frequency independent antenna is to use it in a variety of applications subject to a range of different frequency bands. As per the simulations, this antenna operates from $700MHz$ to $29.9GHz$ and hence can satisfy a massive range of communication spectrum right from somewhere in the middle of the L band ($0.5GHz$ to $1.5GHz$) up to the start of the Ka band ($26GHz$ to $40GHz$) of frequencies.

Also, this antenna is not only about frequency independent behavior. One can effectively change the state of polarization of the radiated wave by reversing the polarity of the signal at feed and changing the face of the antenna.

4.2 Antenna Design

A conventional archimedean spiral antenna, although having a wide frequency bandwidth, has a few shortcomings. The antenna must be fed by a balun since the structure is not impedance matched. The wires might have to run through the spiral arms which can disrupt the electromagnetic characteristics of the structure. Several design options were discussed to improve the feed methods. One inspired from [4] and [6], where the feed is tapered and the structure is a double sided parallel strip line was proposed. The feed becomes a double sided parallel stripline structure

because the arms are on either sides of the substrate and there is no ground plane. In total, exactly two modifications have been done on the conventional design as shown in Figure 2.16 to overcome these shortcomings. This tapering idea evolved into the second modification. The top view of the actual simulation structure in HFSS is shown in Figure 4.1.

The first modification is the change in the position of the arms. One of the arms of the spiral is shifted on the bottom side of the substrate. This gives more space to both the arms on their respective sides of the substrate. Primary advantage of this modification is to simplify feed. One can easily connect a coaxial connector at the center of the spiral with the ground connected to the bottom arm and the signal pin soldered to the top.

Since there is now more space on each side of the substrate, the range of increasing the width of the arms doubles. This is the second modification. As proven in [4], increasing the metal-to-slot ratio decreases the impedance. For a conventional spiral, this metal-to-slot ratio is 1 since it needs to maintain a self-complimentary structure. For this design, this ratio is changed to 4.8 to bring the input impedance in the range of 30Ω to 80Ω. The antenna is designed in Ansys HFSS with the spiral arms as equation based curves. The governing equations are similar to the one discussed in section 2.6 except that they are parameterized in order to suit the HFSS environment.

$$x(t) = (a + b \times t)cos(t) \tag{4.1}$$
$$y(t) = (a + b \times t)sin(t)$$

Here, 't' is the parameter that runs from start to the end of each spiral arm while 'a' and 'b' are constants. The equation for the other arm has an added argument of π in the sinusoidal terms. Top view of this design is shown in Figure 4.1.

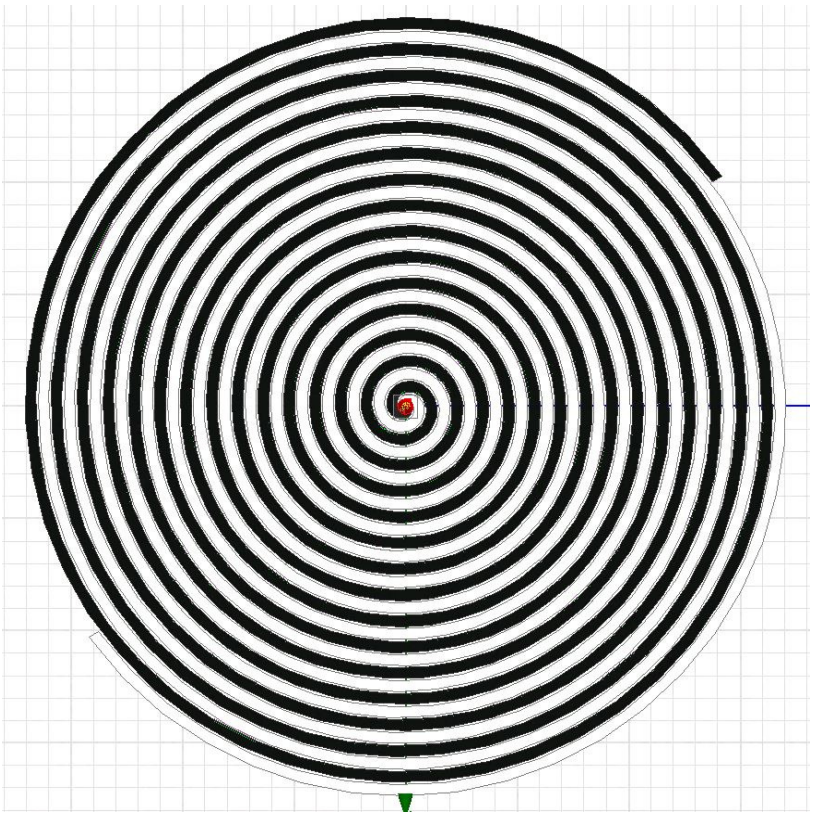

Figure 4.1: Modified Archimedean spiral design in HFSS with one arm on the top side of the substrate (in black) and the other on the bottom side (in white)

For simulation purposes, a coaxial cable is directly connected to the structure. FR-4 is the substrate material used with $\epsilon_r = 4.4$.

4.3 Simulation design and results

Similar simulation settings are used for the Archimedean spiral antenna. With a total of 15 turns on the Spiral, the antenna measures $182.4mm \times 182.4mm$. The arms width is kept at $2.4mm$ while the spacing is at $0.5mm$. An FR-4 substrate with thickness of $0.8mm$ and a dielectric constant of 4.4 is used for all simulations. The width of the substrate is chosen as thin as possible to keep the arms closer for more coupling. Tapering is not done in this design since the antenna is big enough to radiate all the current in air. At the end of the spiral, it is assumed that none of the current reflects back.

As per the simulations done in HFSS, S_{11} is below $-10dB$ across $700MHz$ to $29.9GHz$.

This is shown in Figure 4.2. Z_{11} as shown in Figure 4.3 stays fairly constant throughout the band. The gain patterns for frequencies $1GHz$, $5GHz$, $10GHz$, $15GHz$, $20GHz$ and $30GHz$ are shown in Figures 4.9 through 4.4. The pattern is slightly distorted at $30GHz$ but the gain has remained fairly constant at approximately $6.2dB$ across the band.

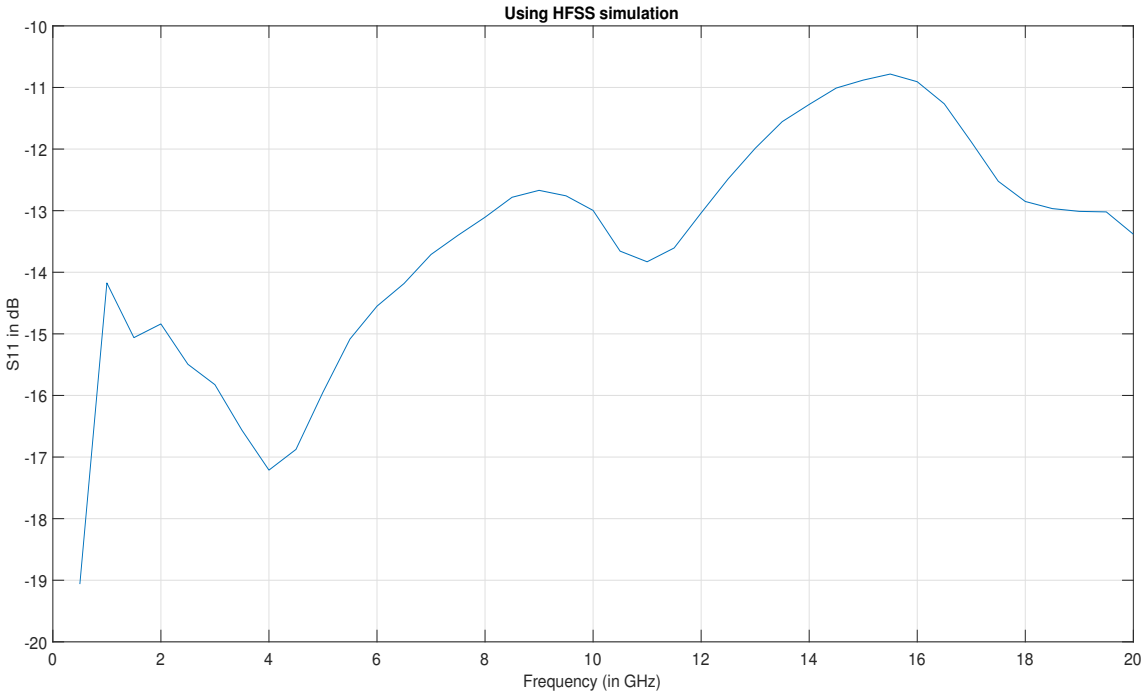

Figure 4.2: Simulated plot of S_{11} of the modified archimedean spiral antenna in HFSS*

The typical shape of the plot for the real and imaginary parts of Z_{11} in Figure 4.3 confirms with the stacked dipole understanding of the spiral. The lumps seen at intervals show resonance at different operating frequencies. It is because of these resonances that the antenna is frequency independent. More such resonances with the correct impedance match, better is the performance of an antenna at those frequencies.

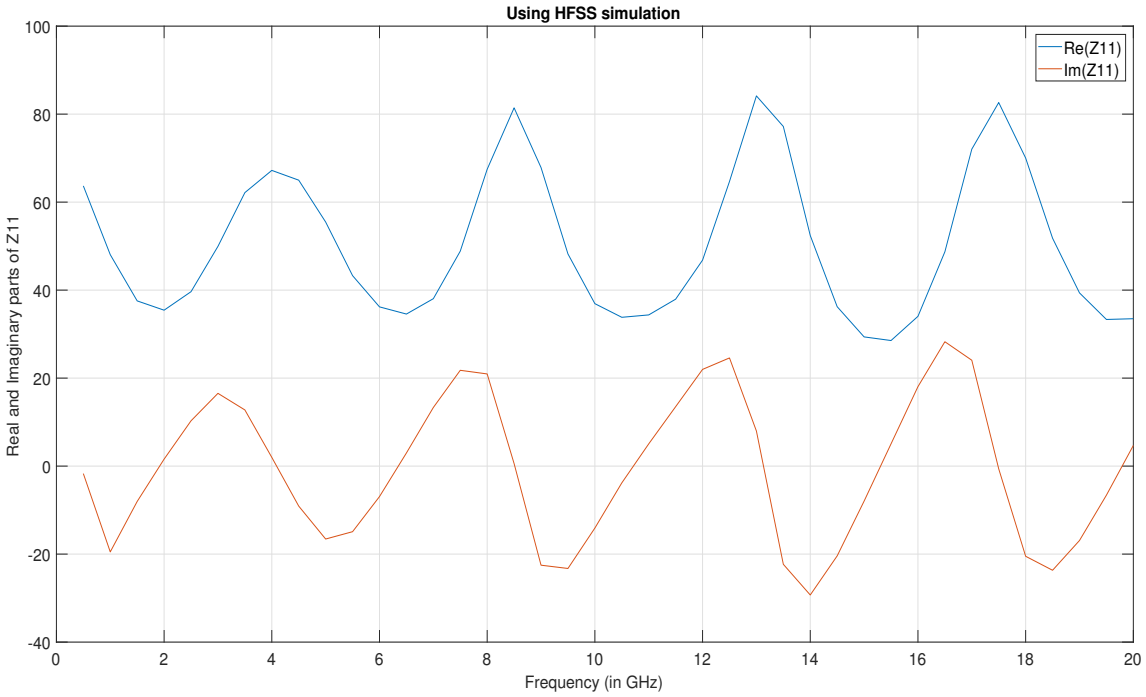

Figure 4.3: Simulated plot of real and imaginary parts of Z_{11} of the modified archimedean spiral antenna in HFSS

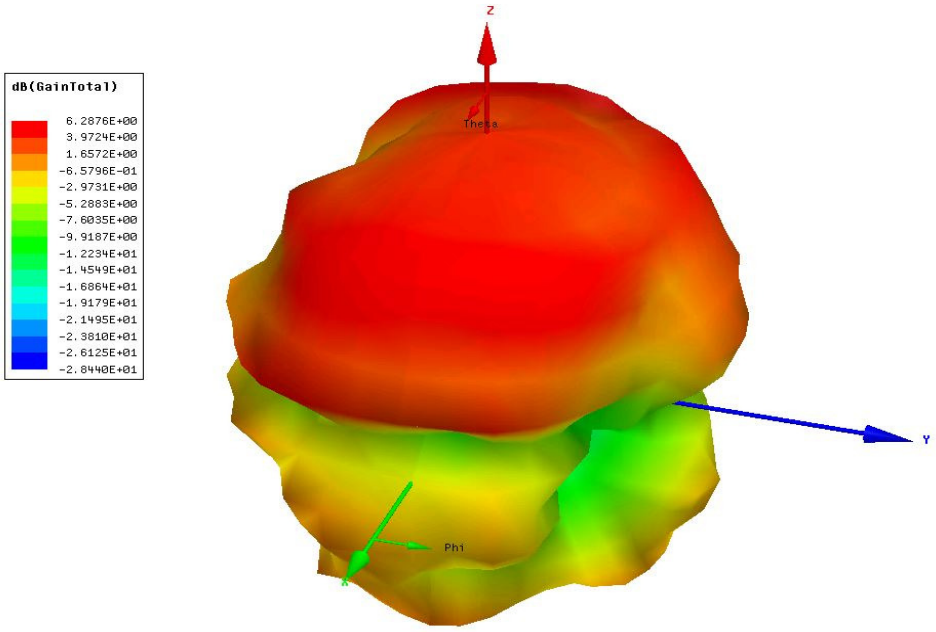

Figure 4.4: Simulated 3D Gain pattern of the modified archimedean spiral antenna at $20GHz$ in HFSS

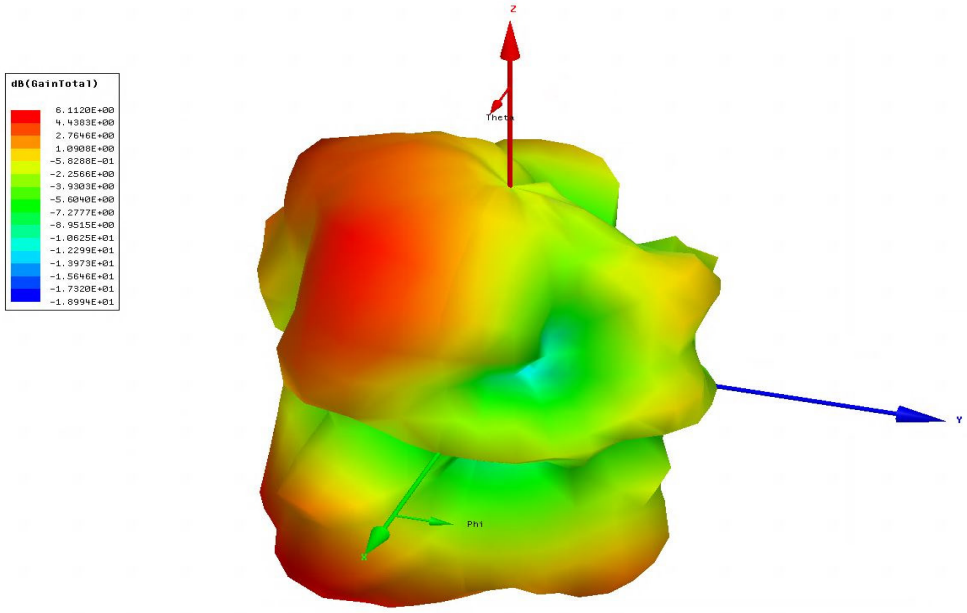

Figure 4.5: Simulated 3D Gain pattern of the modified Spiral antenna at $30GHz$ in HFSS

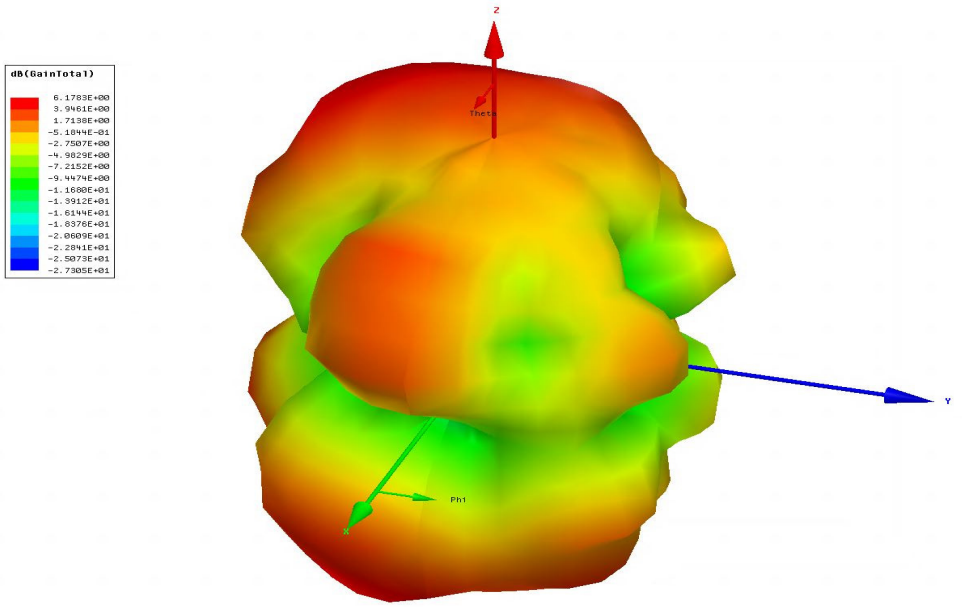

Figure 4.6: Simulated 3D Gain pattern of the modified archimedean spiral antenna at $15GHz$ in HFSS

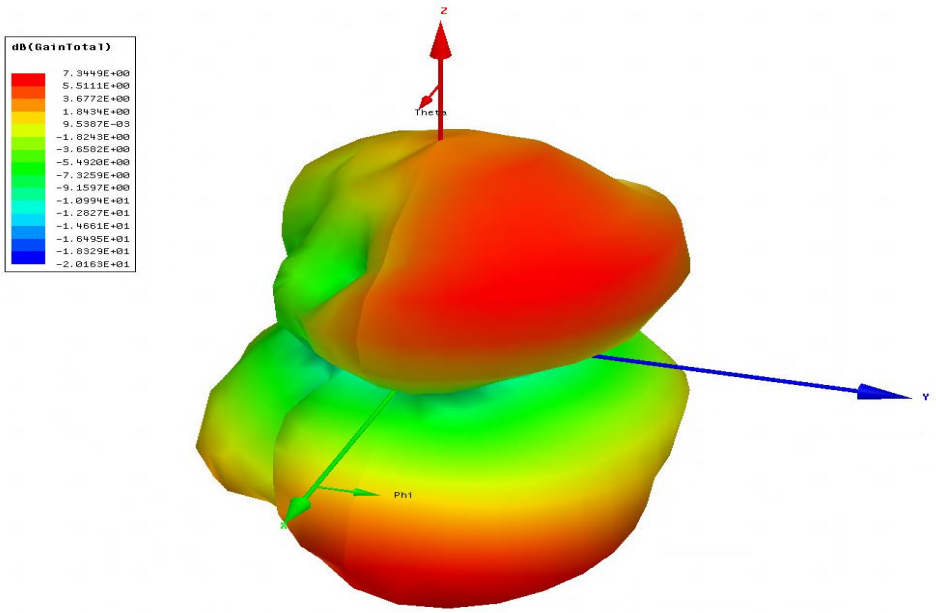

Figure 4.7: Simulated 3D Gain pattern of the modified Spiral antenna at $10GHz$ in HFSS

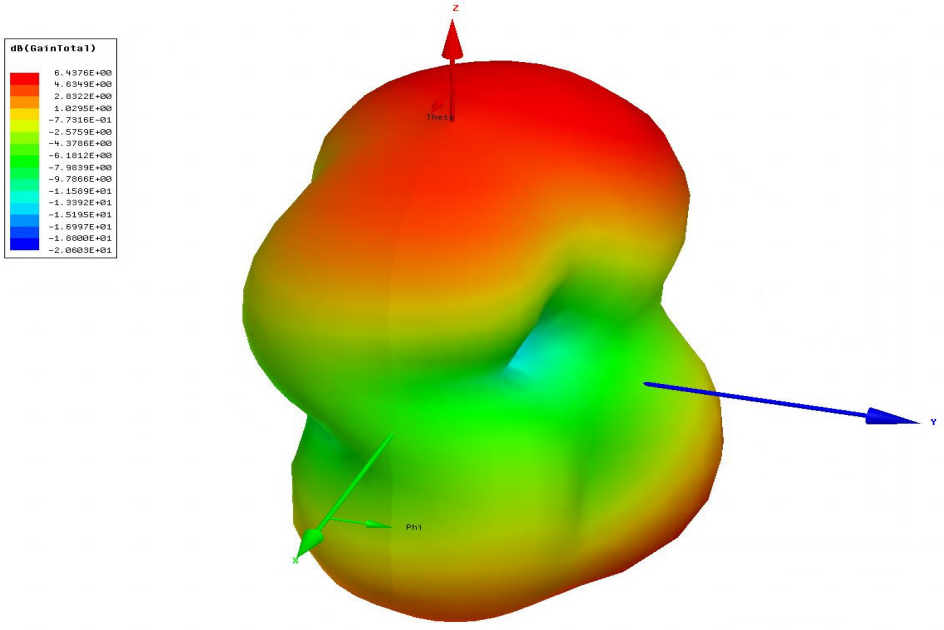

Figure 4.8: Simulated 3D Gain pattern of the modified Spiral antenna at $5GHz$ in HFSS

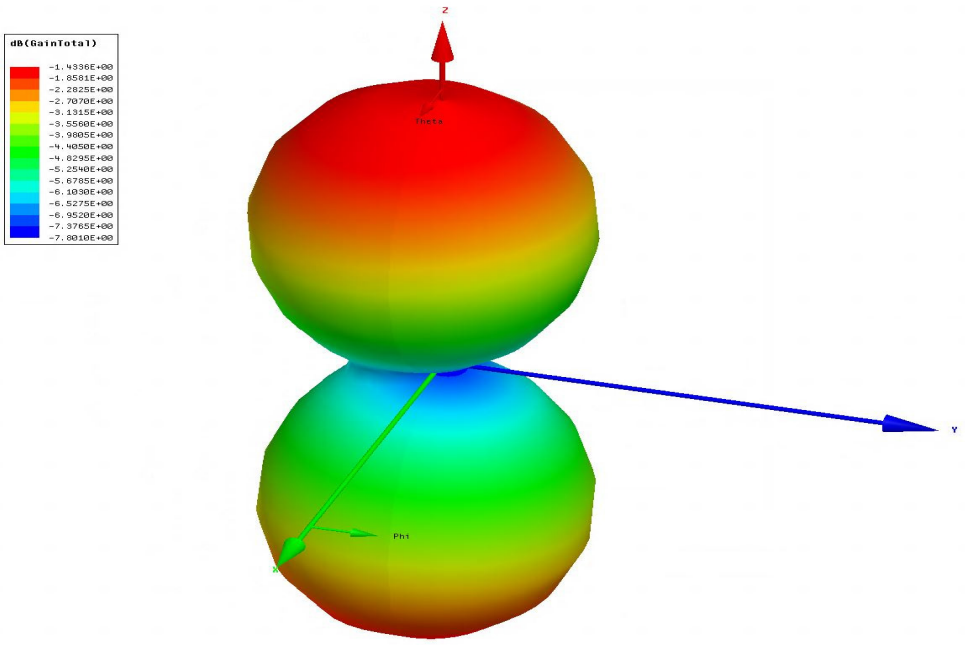

Figure 4.9: Simulated 3D Gain pattern of the modified Spiral antenna at $1GHz$ in HFSS

Noting the turn direction of the antenna structure, the antenna is left-handed circularly polarized. Figure 4.10 shows the radiation pattern of the LHCP plane with a gain of $3.82dB$ in the positive z direction. Figure 4.11 is of particular interest. For the gain on right-handed circular polarization plane, the antenna radiation occurs in the negative z direction. The positive z direction has a gain less than $-1dB$. Figure 4.12 on the Axial ratio tells that the antenna emits circularly polarized waves across the band with less than $2.6dB$ difference between the major and minor axes on the polarization plane. This plot assumes $\theta = 0$ and $\phi = 0$ for keeping the direction on the broadside. It is less than $1dB$ for most of the part of the band, which is quite remarkable.

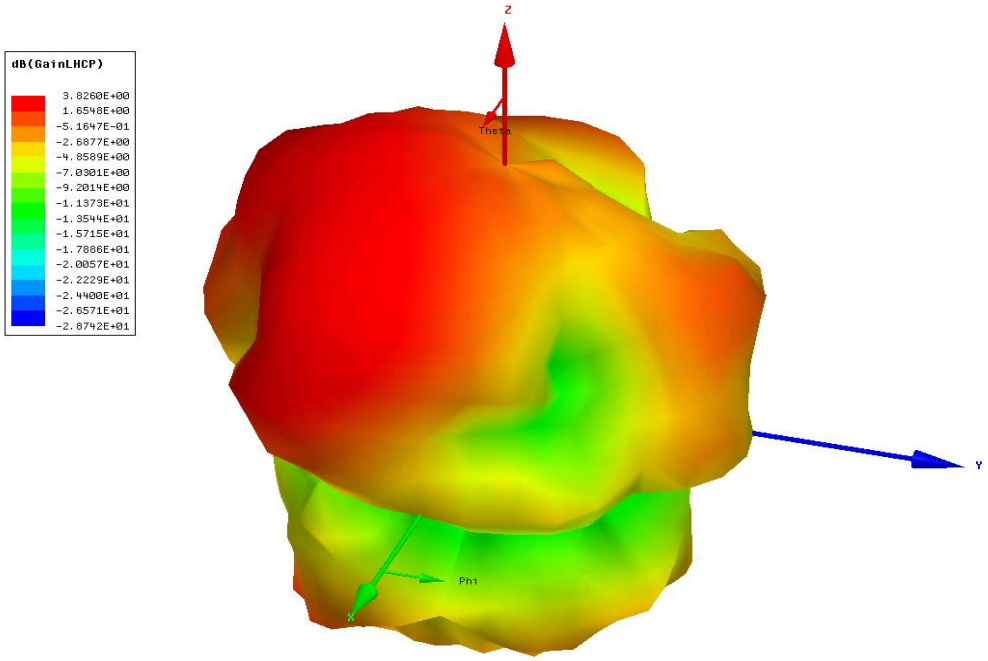

Figure 4.10: 3D Gain pattern of Left-handed circular polarization of the modified Archimedean Spiral antenna on the broadside

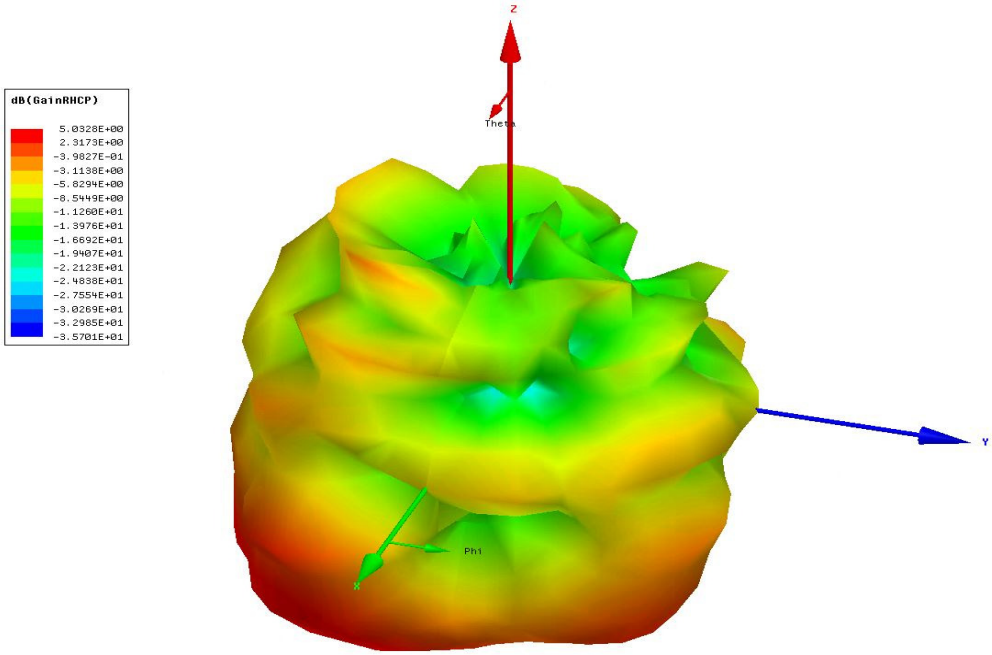

Figure 4.11: 3D Gain pattern of Right-handed circular polarization of the modified Archimedean Spiral antenna on the broadside

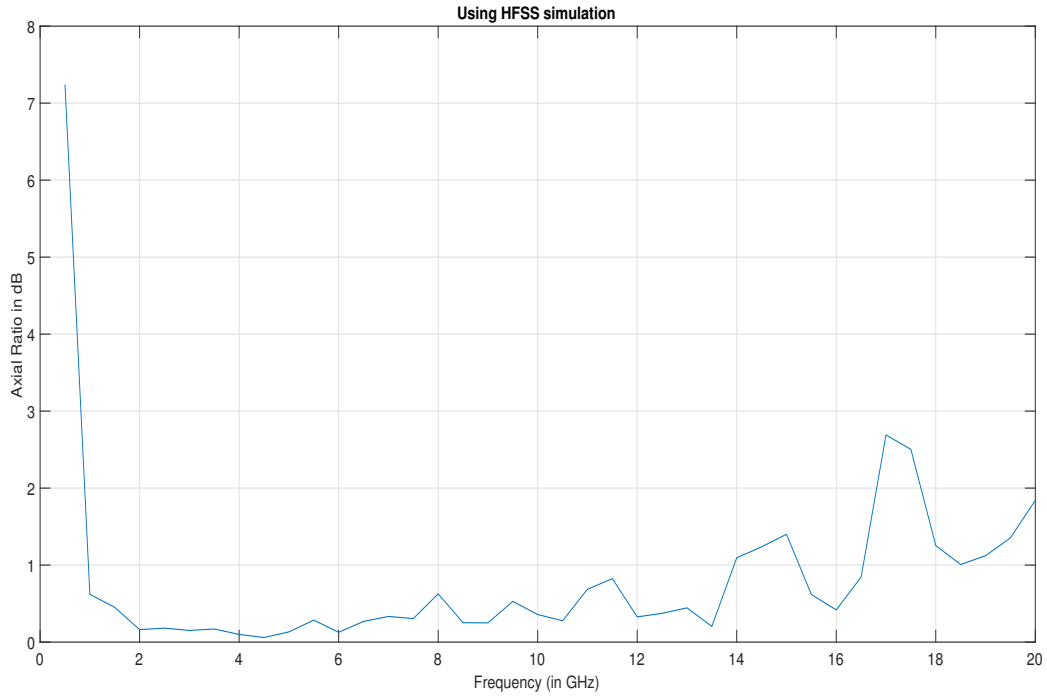

Figure 4.12: Axial Ratio plot in dB on the broadside of the modified Archimedean spiral with respect to frequency

4.4 Measured data

Measurements are done on Anritsu MS46322A Vector Network Analyser. The fabricated Archimedean spiral antenna is shown in Figures 4.13 and 4.14 with both its faces. Since the structure has an average input impedance of 50Ω across the band, a coaxial connector is directly soldered on the substrate.

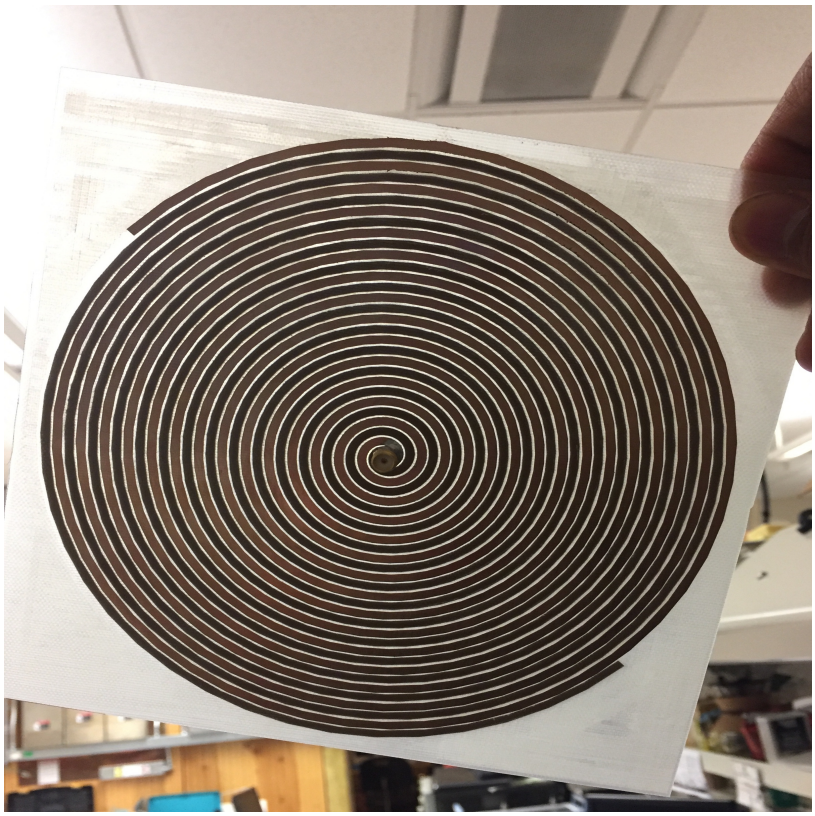

Figure 4.13: Fabricated design of the modified Archimedean Spiral antenna in air showing the top and the bottom arms

As it is evidently seen in Figure 4.13, the structure requires no balun at the input. The coaxial connector is directly attached to the center of the archimedean spiral. The width to gap ratio has changed the input impedance of the antenna close to 50Ω. The coaxial connector used in the Figure is through-hole type and has a bandwidth of up to $19GHz$. With better fabrication efficiency and changing the connector to a surface mount type, the antenna is believed to operate at higher bandwidths.

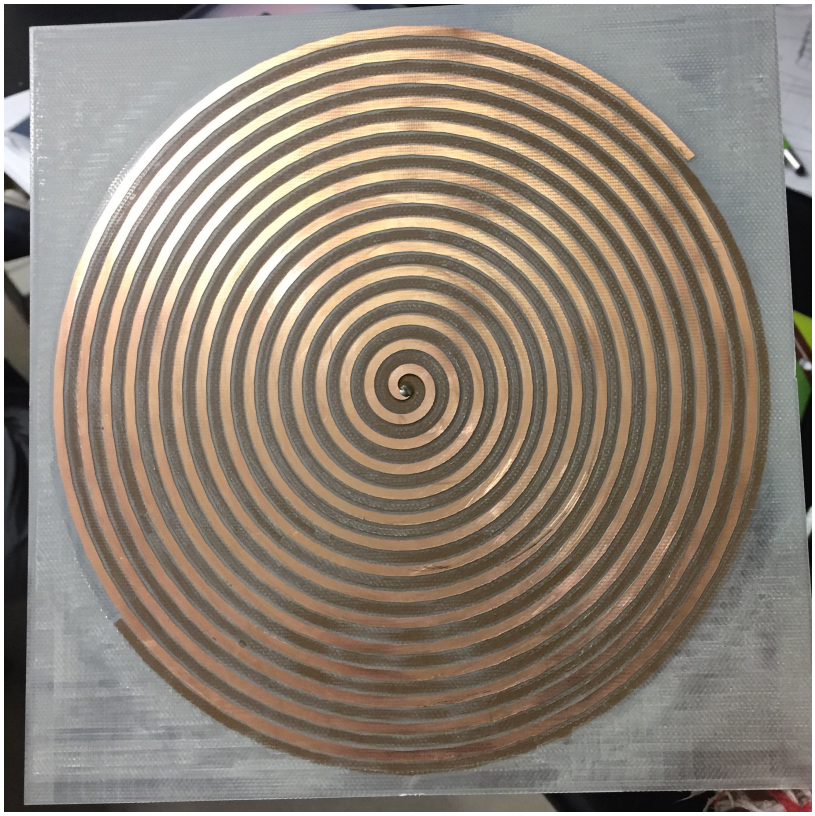

Figure 4.14: Top face view of the modified Archimedean Spiral antenna

From the top face, only one arm is seen, as shown in Figure 4.14. The feed is not seen here since it is on the bottom face. The width of both the arms have been kept constant from the beginning till the end of the design. Tapering the arms at the ends may improve S_{11} performance since this may reduce the amount of reflected current.

The measured plot for S_{11} across the band is shown in Figure 4.15. It is interesting to note that the plot crosses the $-10dB$ mark near $20GHz$ instead of $30GHz$ seen in simulation. This is because the coaxial connector used in the antenna design had a bandwidth limitation at approximately $19GHz$. This plot would have had wider bandwidth if an appropriate connector with S_{11} less than $-10dB$ across the band till $30GHz$ is used.

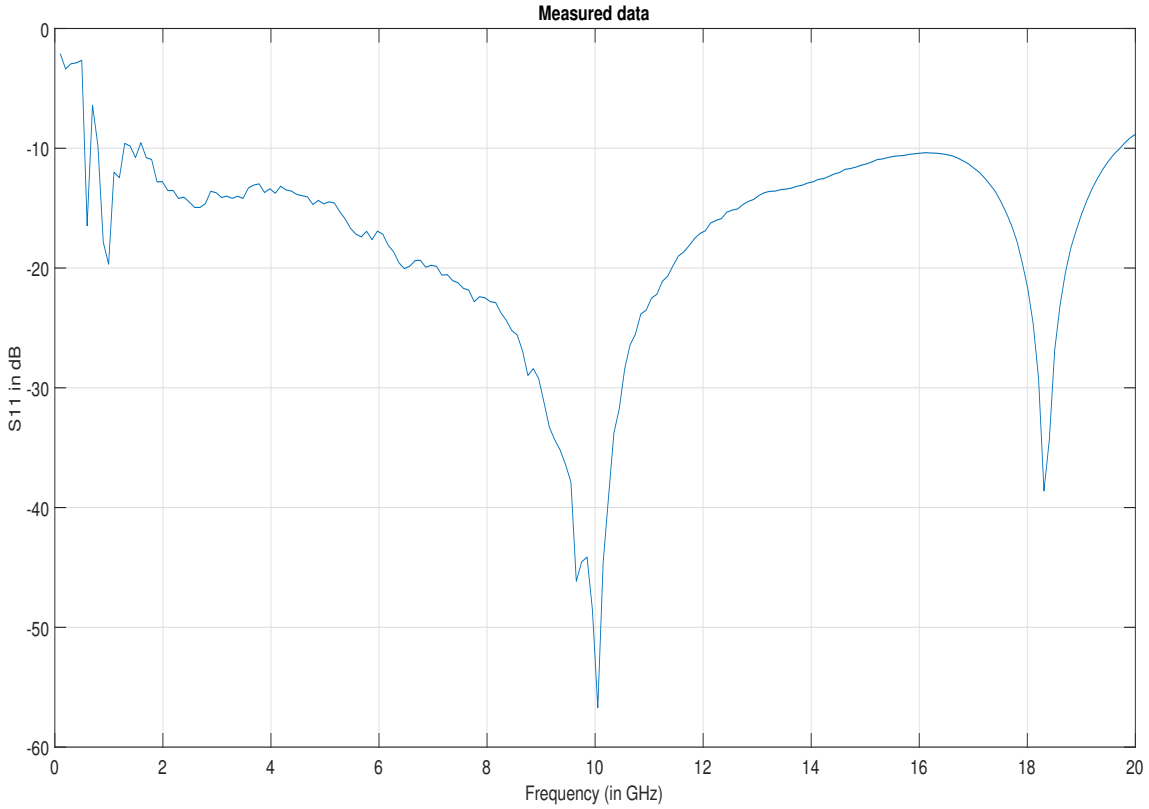

Figure 4.15: Measured S_{11} of the modified Archimedean spiral antenna

The plot has S_{11} more than $-10dB$ in the lower frequency range where it is fluctuating rapidly. The reason behind this transience is not clear. Also the lowest value of S_{11} is observed at around $10GHz$ which is not seen in simulations. It is suspected that the connector impedance characteristic at that frequency might be a reason.

4.5 Conclusion

The technique of offsetting the arms of the spiral vertically improved the impedance characteristics of the antenna over the complete bandwidth of interest and made the feed simpler. The radiation characteristics were not affected by this modification.

CHAPTER 5: CONCLUSIONS AND FUTURE WORK

Two classes of antennas- the narrow band patch antenna array and the frequency independent Archimedean spiral have been shown to gain advancements in terms of bandwidth, simplicity in the feed and a novel approach to the polarization of the radiated wave. This effort is a proof that simple design ideas can lead to extremely useful inventions. The idea of encrypted polarization is not only boasts a breakthrough in terms of data security, but it also approves a simple implementation. The proposal for using an antenna as a filter alters the way antennas fit in a conventional transceiver system. Antenna, when used as radiative filter, can be used at an intermediate stage, just as a traditional filter. This approach can change the way antennas are perceived. From what is observed during this development seems to be only a start of a remarkable technology in the future. The modified archimedean spiral antenna is one which has a simple feed and a satisfactory far-field radiation pattern for the complete range of frequencies from $700MHz$ to $29GHz$, reaching a $40:1$ bandwidth. Wider arms helped bring down the input impedance near 50Ω.

Having two ports to the patch antenna array introduced the possibility of using the structure as a two port network. Along with using the antenna as a filter which radiates, one can also change the polarization of the radiated wave on the fly. This concept can be extended to other antenna types or different patch shapes.

As a part of future work, one can attempt to prove the concept of encrypted polarization by keeping two similar patch antenna arrays on the transmitting and the receiving end. One then will have to synchronously match the port switching frequency of both the antennas in order to receive the complete signal. The idea of offsetting the arms vertically can be tried on other frequency independent designs

like the equiangular spiral or the log-periodic antenna. It has been shown that for a microstrip patch array, the radiated beams can be switched using a butler matrix [17]. Although, there is no change in polarization for these beams but it can be useful as a future work on the antenna developed here.

REFERENCES

[1] J. Volakis, *Antenna Engineering Handbook, Fourth Edition*. McGraw-Hill Education, 2007.

[2] B. Shanmugam and S. K. Sharma, "Investigations on a novel modified archimedean spiral antenna," in *2011 IEEE International Symposium on Antennas and Propagation (APSURSI)*, pp. 1225–1228, July 2011.

[3] V. Rumsey, "Frequency independent antennas," in *1958 IRE International Convention Record*, vol. 5, pp. 114–118, March 1957.

[4] D. Li, L. Li, Z. Li, and G. Ou, "Four-arm spiral antenna fed by tapered transmission line," *IEEE Antennas and Wireless Propagation Letters*, vol. 16, pp. 62–65, 2017.

[5] A. M. Shire and F. C. Seman, "Effects of dielectric substrate on performance of uwb archimedean spiral antenna," in *2013 IEEE International Conference on Space Science and Communication (IconSpace)*, pp. 412–415, July 2013.

[6] Y. Li, Q. Xue, E. K. N. Yung, and Y. Long, "The backfire-to-broadside symmetrical beam-scanning periodic offset microstrip antenna," *IEEE Transactions on Antennas and Propagation*, vol. 58, pp. 3499–3504, Nov 2010.

[7] H. Sun, Y. X. Guo, and Z. Wang, "60-ghz circularly polarized u-slot patch antenna array on ltcc," *IEEE Transactions on Antennas and Propagation*, vol. 61, pp. 430–435, Jan 2013.

[8] Z. Chen and S. Otto, "A taper optimization for pattern synthesis of microstrip series-fed patch array antennas," in *2009 European Wireless Technology Conference*, pp. 160–163, Sept 2009.

[9] D. M. Pozar and D. H. Schaubert, "Comparison of three series fed microstrip array geometries," in *Proceedings of IEEE Antennas and Propagation Society International Symposium*, pp. 728–731 vol.2, June 1993.

[10] C. A. Balanis, *Antenna Theory - Analysis And Design*. Hoboken, New Jersey: John Wiley Sons, Inc., 2005.

[11] K.-F. Lee, K.-M. Luk, and J. S. Dahele, "Characteristics of the equilateral triangular patch antenna," *IEEE Transactions on Antennas and Propagation*, vol. 36, pp. 1510–1518, Nov 1988.

[12] Y. J. Guo, A. Paez, R. A. Sadeghzadeh, and S. K. Barton, "A circular patch antenna for radio lan's," *IEEE Transactions on Antennas and Propagation*, vol. 45, pp. 177–178, Jan 1997.

[13] W.-S. Chen, C.-K. Wu, and K.-L. Wong, "Novel compact circularly polarized square microstrip antenna," *IEEE Transactions on Antennas and Propagation*, vol. 49, pp. 340–342, Mar 2001.

[14] "Ieee standard for definitions of terms for antennas," *IEEE Std 145-2013 (Revision of IEEE Std 145-1993)*, pp. 1–50, March 2014.

[15] D. M. Pozar, *Microwave Engineering, 3rd Ed.* New York, NY: Wiley, 2005.

[16] "U bend title," *IEEE Std 145-2013 (Revision of IEEE Std 145-1993)*, pp. 1–50, March 2014.

[17] C. H. Tseng, C. J. Chen, and T. H. Chu, "A low-cost 60-ghz switched-beam patch antenna array with butler matrix network," *IEEE Antennas and Wireless Propagation Letters*, vol. 7, pp. 432–435, 2008.

VITA

Dip Thakar was born on 17^{th} February 1991 in Vadodara, Gujarat, India. He earned his bachelors degree in Electronics and Communication Engineering from Gujarat Technological University (GTU) in 2013 and masters degree in Electrical and Electronics engineering from University of North Carolina at Charlotte (UNCC). He has worked for Matrix ComSec Pvt. Ltd. for two years as a hardware design engineer. Currently he is an RF product engineer at Analog Devices, Inc in North Carolina, USA.